



ARCHIVIO ISTITUZIONALE DELLA RICERCA

Alma Mater Studiorum Università di Bologna Archivio istituzionale della ricerca

Thermal Growth of Au-Fe Heterometallic Carbonyl Clusters Containing N-Heterocyclic Carbene and Phosphine Ligands

This is the final peer-reviewed author's accepted manuscript (postprint) of the following publication:

Published Version:

Thermal Growth of Au-Fe Heterometallic Carbonyl Clusters Containing N-Heterocyclic Carbene and Phosphine Ligands / Berti B.; Bortoluzzi M.; Cesari C.; Femoni C.; Iapalucci M.C.; Mazzoni R.; Vacca F.; Zacchini S.. - In: INORGANIC CHEMISTRY. - ISSN 0020-1669. - STAMPA. - 59:4(2020), pp. 2228-2240. [10.1021/acs.inorgchem.9b02912]

This version is available at: <https://hdl.handle.net/11585/763790> since: 2020-07-01

Published:

DOI: <http://doi.org/10.1021/acs.inorgchem.9b02912>

Terms of use:

Some rights reserved. The terms and conditions for the reuse of this version of the manuscript are specified in the publishing policy. For all terms of use and more information see the publisher's website.

(Article begins on next page)

This item was downloaded from IRIS Università di Bologna (<https://cris.unibo.it/>).
When citing, please refer to the published version.

This is the final peer-reviewed accepted manuscript of:

B. Berti, M. Bortoluzzi, C. Cesari, C. Femoni, M. C. Iapalucci, R. Mazzoni, F. Vacca, S. Zacchini, "Thermal Growth of Au-Fe Heterometallic Carbonyl Clusters Containing N-Heterocyclic Carbene and Phosphine Ligands", *Inorg. Chem.* **2020**, *59*, 2228-2240

The final published version is available online at:

<https://doi.org/10.1021/acs.inorgchem.9b02912>

Rights / License: Licenza per Accesso Aperto. Creative Commons Attribuzione - Non commerciale - Non opere derivate 4.0 (CCBYNCND)

The terms and conditions for the reuse of this version of the manuscript are specified in the publishing policy. For all terms of use and more information see the publisher's website.

This item was downloaded from IRIS Università di Bologna (<https://cris.unibo.it/>)

When citing, please refer to the published version.

Thermal Growth of Au-Fe Heterometallic Carbonyl Clusters Containing *N*-Heterocyclic Carbene and Phosphine Ligands

Beatrice Berti,[†] Marco Bortoluzzi,[‡] Cristiana Cesari,[†] Cristina Femoni,[†] Maria Carmela Iapalucci,[†]
Rita Mazzoni,[†] Federico Vacca,[†] and Stefano Zacchini*,[†]

[†] Dipartimento di Chimica Industriale "Toso Montanari", University of Bologna, Viale
Risorgimento 4, I-40136 Bologna Italy. E-mail: stefano.zacchini@unibo.it; Web:
<https://www.unibo.it/sitoweb/stefano.zacchini/en>; Tel: +39 051 2093711.

[‡] Dipartimento di Scienze Molecolari e Nanosistemi, Ca' Foscari University of Venice, Via Torino
155 – 30175 Mestre (Ve), Italy.

ABSTRACT: The thermal reactions of [NEt₄][Fe(CO)₄(AuNHC)] (NHC = IMes, [NEt₄][**1**]; IPr, [NEt₄][**2**]; IMes = C₃N₂H₂(C₆H₂Me₃)₂; IPr = C₃N₂H₂(C₆H₃ⁱPr₂)₂), Fe(CO)₄(AuNHC)₂ (NHC = IMes, **3**; IPr, **4**), Fe(CO)₄(AuIMes)(AuIPr) (**5**) and Fe(CO)₄(AuNHC)(AuPPh₃) (NHC = IMes, **6**; IPr, **7**) were investigated in different solvents (CH₂Cl₂, CH₃CN, dmf, dmsO) and at different temperatures (50-160 °C) in the attempt to obtain higher nuclearity clusters. **1** and **2** completely decomposed in refluxing CH₂Cl₂ resulting in [Fe₂(CO)₈(AuNHC)]⁻ (NHC = IMes, **10**; IPr, **11**). Traces of [Fe₃(CO)₁₀(CCH₃)]⁻ (**12**) were obtained as side-product. Conversely, **6** decomposed in refluxing CH₃CN affording the new cluster [Au₃{Fe(CO)₄}₂(PPh₃)₂]⁻ (**15**). The relative stability of the two isomers found in the solid state structure of **15** was computationally investigated. **4** was very stable and only after prolonged heating above 150 °C in dmsO limited decomposition was observed, affording small amounts of [Fe₃S(CO)₉]²⁻ (**9**), [HFe(CO)₄]⁻ (**16**) and [Au₁₆S{Fe(CO)₄}₄(IPr)₄]ⁿ⁺ (**17**). A dicationic nature for **17** was proposed on the basis of DFT calculations. All the other reactions examined led to species which were previously reported. The molecular structures of the new clusters **11**, **12**, **15** and **17** were determined by means of single crystal X-ray diffraction as their [NEt₄][**11**]·1.5toluene, [Au(IMes)₂][**15**]·0.67CH₂Cl₂, [NEt₄][**12**] and [**17**][BF₄]_n·solv salts.

This item was downloaded from IRIS Università di Bologna (<https://cris.unibo.it/>)

When citing, please refer to the published version.

1. Introduction

The $\text{Fe}(\text{CO})_4$ group was a very versatile fragment for stabilizing gold clusters.¹ These included low nuclearity complexes such as $\text{Fe}(\text{CO})_4(\text{AuPPh}_3)_2$,² $\text{Fe}(\text{CO})_4(\text{AuNHC})_2$ (NHC = IMes, IPr, IBu; IMes = $\text{C}_3\text{N}_2\text{H}_2(\text{C}_6\text{H}_2\text{Me}_3)_2$; IPr = $\text{C}_3\text{N}_2\text{H}_2(\text{C}_6\text{H}_3\text{Pr}_2)_2$; IBu = $\text{C}_3\text{N}_2\text{H}_2(\text{CMe}_3)_2$),³ and $[\text{Fe}(\text{CO})_4(\text{AuNHC})]^-$,⁴ as well as 1-D and 2-D gold clusters, such as $[\text{Au}_3\text{Fe}_2(\text{CO})_8(\text{IMes})_2]^-$,³ $[\text{Au}_3\text{Fe}(\text{CO})_4(\text{dppm})_2]^+$ (dppm = $\text{Ph}_2\text{PCH}_2\text{PPh}_2$),⁵ $[\text{Au}_3\text{Fe}_2(\text{CO})_8(\text{dppm})]^-$,⁶ $[\text{Au}_3\{\text{Fe}(\text{CO})_4\}_3]^{3-}$,⁷ $[\text{Au}_4\{\text{Fe}(\text{CO})_4\}_4]^{4+}$,⁸ $[\text{Au}_5\text{Fe}_4(\text{CO})_{16}]^{3-}$,⁹ $[\text{Au}_5\text{Fe}_2(\text{CO})_8(\text{dppm})_2]^+$,⁶ and $\text{Au}_8\text{Fe}_4(\text{CO})_{16}(\text{dppe})_4$ (dppe = $\text{Ph}_2\text{PCH}_2\text{CH}_2\text{PPh}_2$).¹⁰ These clusters could be viewed as composed of $[\text{Fe}(\text{CO})_4]^{2-}$ moieties and Au(I) ions, containing in some cases additional NHC and/or phosphine ligands. The general strategy for their syntheses was the reaction of the Colman's reagent $\text{Na}_2[\text{Fe}(\text{CO})_4]\cdot 2\text{thf}$ with Au(I) complexes such as $\text{Au}(\text{Et}_2\text{S})\text{Cl}$, $[\text{AuBr}_2]^-$, $\text{Au}(\text{PPh}_3)\text{Cl}$, $\text{Au}(\text{NHC})\text{Cl}$, $\text{Au}_2(\text{dppm})\text{Cl}_2$ and $\text{Au}_2(\text{dppe})\text{Cl}_2$.

In addition 3-D metalloid Fe-Au clusters were obtained from the redox condensation of $[\text{Fe}_3(\text{CO})_{11}]^{2-}$ and $[\text{AuCl}_4]^-$. This category included Au-Fe-CO molecular nanoclusters such as $[\text{Au}_{21}\text{Fe}_{10}(\text{CO})_{40}]^{5-}$, $[\text{Au}_{22}\text{Fe}_{12}(\text{CO})_{48}]^{6-}$, $[\text{Au}_{28}\text{Fe}_{14}(\text{CO})_{52}]^{8-}$ and $[\text{Au}_{34}\text{Fe}_{14}(\text{CO})_{50}]^{8-}$, stabilised by $\text{Fe}(\text{CO})_4$ and $\text{Fe}(\text{CO})_3$ groups present on their surface.⁹ The Au atoms within their Au_n core displayed a formal oxidation state comprised between +1 and 0. Linear Fe-Au-Fe staple motives, reminiscent of the very well known S-Au-S staple motives found in Au-thiolate nanoclusters, were present on the surface of these organometallic Au-Fe carbonyl clusters.^{9,11,12}

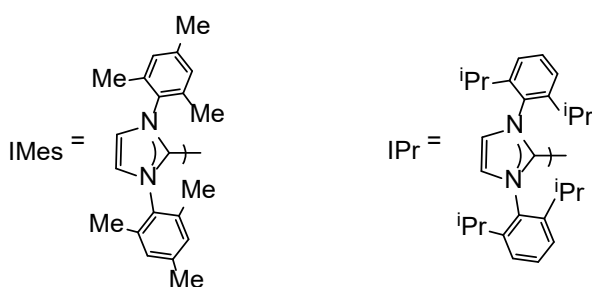
The interest for atomically precise (molecular) gold nanoclusters has incredibly grown in the recent years, because of their fundamental aspects and properties as well as possible applications.¹³⁻¹⁹ Thiolate and phosphine ligands were widely employed for the preparation of molecular gold nanoclusters, but other ligands,²⁰⁻²² including organometallic fragments, might be employed. In this sense, the combination of $\text{Fe}(\text{CO})_4$, NHC and phosphine ligands might be an interesting approach for the growth of new gold clusters. In addition, Au-Fe carbonyl clusters were also useful platforms for the study of intra-molecular aurophilic interactions.^{1,7,11,23-25} In view of this broad interest for gold clusters and aurophilic interactions, the preparation of gold-containing molecular clusters of increasing sizes is still a fascinating challenge.

Thermal reactions of low nuclearity precursors might be an alternative to redox condensation for the preparation of higher nuclearity Fe-Au carbonyl clusters. Indeed, it was recently reported that the thermal treatment of $\text{Fe}(\text{CO})_4(\text{AuIMes})_2$ resulted in $[\text{Au}_3\{\text{Fe}(\text{CO})_4\}_3]^{3-}$ or

This item was downloaded from IRIS Università di Bologna (<https://cris.unibo.it/>)

When citing, please refer to the published version.

$[\text{Au}_3\text{Fe}_2(\text{CO})_8(\text{IMes})_2]^-$ depending of the experimental conditions.^{3,7} In both cases, the reactions involved ionization of the neutral precursors and rearrangement of the ligands, with retention of the original oxidation states -2 and +1 for Fe and Au, respectively. It is also worth noting that thermal reaction of $\text{Fe}(\text{CO})_4(\text{AuIMes})_2$ was the only synthetic approach viable for the $[\text{Au}_3\{\text{Fe}(\text{CO})_4\}_3]^{3-}$ trinuclear compound, whereas the direct reaction of $\text{Na}_2[\text{Fe}(\text{CO})_4]\cdot 2\text{thf}$ with $[\text{AuBr}_2]^-$ afforded selectively the $[\text{Au}_4\{\text{Fe}(\text{CO})_4\}_4]^{4-}$ tetranuclear compound.⁸ These preliminary results prompted us to systematically study the thermal reactions of low nuclearity mono-anionic and neutral precursors such as $[\text{NEt}_4][\text{Fe}(\text{CO})_4(\text{AuNHC})]$ (NHC = IMes, $[\text{NEt}_4][\mathbf{1}]$; IPr, $[\text{NEt}_4][\mathbf{2}]$; IMes = $\text{C}_3\text{N}_2\text{H}_2(\text{C}_6\text{H}_2\text{Me}_3)_2$; IPr = $\text{C}_3\text{N}_2\text{H}_2(\text{C}_6\text{H}_3\text{iPr}_2)_2$, Scheme 1), $\text{Fe}(\text{CO})_4(\text{AuNHC})_2$ (NHC = IMes, $\mathbf{3}$; IPr, $\mathbf{4}$), $\text{Fe}(\text{CO})_4(\text{AuIMes})(\text{AuIPr})$ ($\mathbf{5}$) and $\text{Fe}(\text{CO})_4(\text{AuNHC})(\text{AuPPh}_3)$ (NHC = IMes, $\mathbf{6}$; IPr, $\mathbf{7}$). The outcomes of the different reactions are reported herein, supported by a computational investigation on new products characterized by unusual isomerism and bond structure.



Scheme 1. The IMes and IPr ligands.

2. Results and Discussion

The thermal reactions of the complexes $\mathbf{1-7}$ were investigated aiming at obtaining higher nuclearity species. As a general strategy, $\mathbf{1-7}$ were heated in different solvents (CH_2Cl_2 , CH_3CN , dmf, dmsO) at temperatures in the range 50-160 °C monitoring the time-evolution of the reactions by IR spectroscopy in the ν_{CO} region. Anionic compounds were examined as $[\text{NEt}_4]^+$ salts. The crude reaction mixtures were recovered after removal of the organic solvent under reduced pressure or, in the case of dmf and dmsO as solvent, by precipitation with H_2O in the presence of a suitable tetra-alkyl-ammonium salt. The solid residue was extracted with solvents of increasing polarity in the attempt to separate the products from the crude reaction mixtures. Further details can be found in the Experimental Section. All the results obtained were summarized in Scheme 2. The new results herein obtained can be summarized as follow:

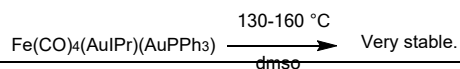
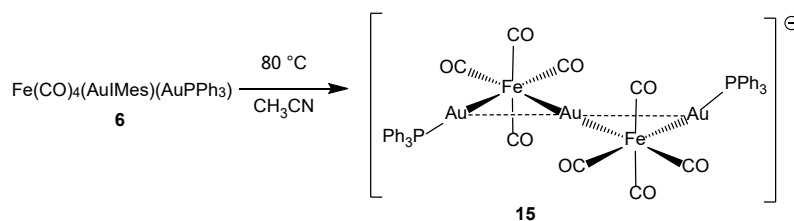
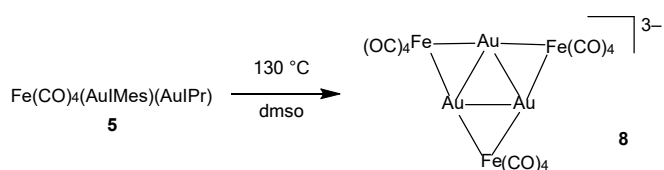
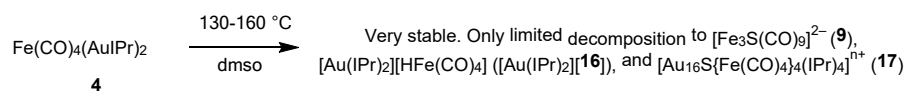
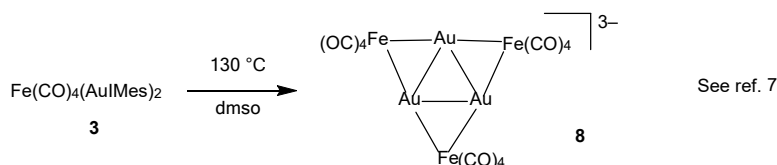
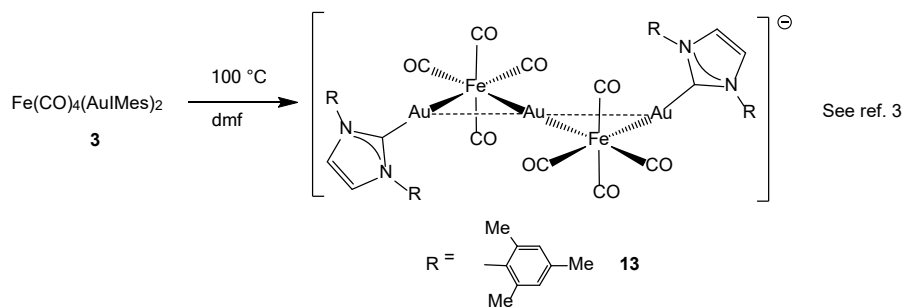
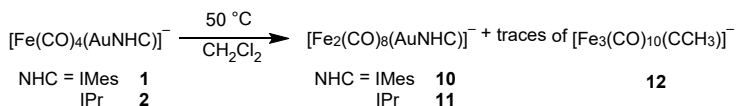
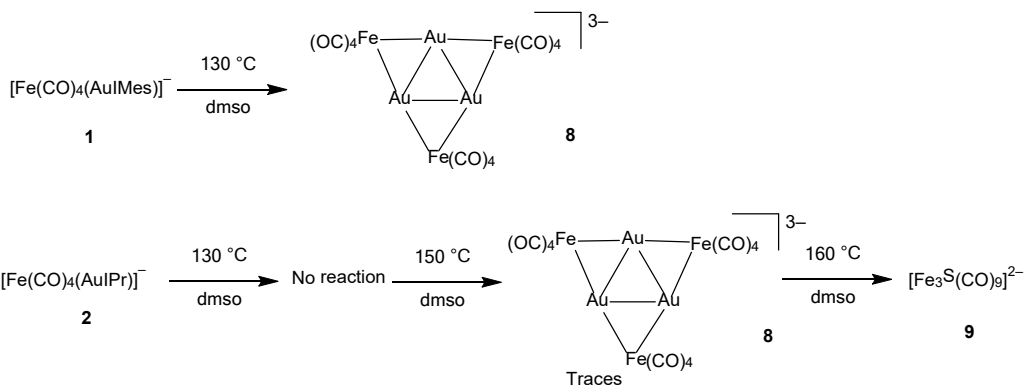
This item was downloaded from IRIS Università di Bologna (<https://cris.unibo.it/>)

When citing, please refer to the published version.

- 1) Heating the mono-anions **1** and **2** as $[\text{NEt}_4]^+$ salts in CH_2Cl_2 at refluxing temperature resulted in the formation of $[\text{Fe}_2(\text{CO})_8(\text{AuNHC})]^-$ (NHC = IMes, **10**; IPr, **11**). Traces of $[\text{Fe}_3(\text{CO})_{10}(\text{CCH}_3)]^-$ (**12**) were obtained as side-product. These represented an interesting addition to the limited number of compounds with the $\text{Fe}_2(\text{CO})_6(\mu\text{-CO})_2$ unit (Section 2.1)
- 2) The thermal decomposition of **6** in CH_3CN at $80\text{ }^\circ\text{C}$ afforded the larger $[\text{Au}_3\{\text{Fe}(\text{CO})_4\}_2(\text{PPh}_3)_2]^-$ (**15**) cluster which was present as two isomers in the solid state structure (Section 2.2).
- 3) **4** was only partially decomposed after prolonged heating in dmsO at $130\text{-}160\text{ }^\circ\text{C}$ resulting in a mixture of $[\text{Fe}_3\text{S}(\text{CO})_9]^{2-}$ (**9**), $[\text{HFe}(\text{CO})_4]^-$ (**16**) and $[\text{Au}_{16}\text{S}\{\text{Fe}(\text{CO})_4\}_4(\text{IPr})_4]^{n+}$ (**17**). Compound **17** was rather interesting because it was a high nuclearity Au-cluster containing an interstitial $\mu_{12}\text{-S}$ atom stabilized on the surface by $\text{Fe}(\text{CO})_4$ fragments and IPr ligands (Section 2.3).

This item was downloaded from IRIS Università di Bologna (<https://cris.unibo.it/>)

When citing, please refer to the published version.

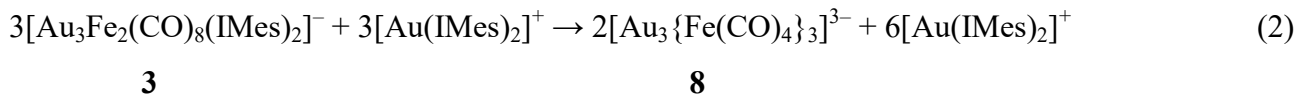
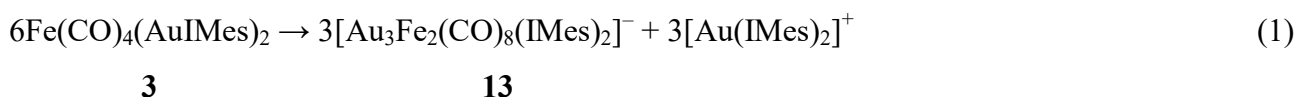


This item was downloaded from IRIS Università di Bologna (<https://cris.unibo.it/>)

When citing, please refer to the published version.

Scheme 2. Thermal reactions of 1-7.

The other reactions studied led to compounds which were previously published and, therefore, they will not be discussed any further.^{3,4,7} These included $[\text{Au}_3\{\text{Fe}(\text{CO})_4\}_3]^{3-}$ (**8**),⁷ $[\text{Fe}_3\text{S}(\text{CO})_9]^{2-}$ (**9**)²⁶ and $[\text{Au}_3\text{Fe}_2(\text{CO})_8(\text{IMes})_2]^-$ (**13**).³ In particular, **8** was obtained as the main product of several reactions. We reported the synthesis of **8** by the thermal decomposition of **3** in dmsO at 130°C in a previous communication.⁷ As summarized in Scheme 2, **8** could be obtained also by thermal treatment of **1**, **2** and **5**. **13** was obtained by the thermal reaction of **3** at lower temperatures ($\leq 100^\circ\text{C}$) in dmf or dmsO,³ whereas **8** was formed at higher temperatures. The computed Gibbs energy variations (C-PCM/PBEh-3c calculations) for the reactions (1) and (2) were -13.1 and -23.1 kcal mol⁻¹, respectively, and suggested that the formation of $[\text{Au}(\text{IMes})_2]^+$ was the driving force. As a general comment on Scheme 2, IPr-containing species were far more thermally stable than IMes-ones.



2.1 Syntheses and characterization of $[\text{Fe}_2(\text{CO})_8(\text{AuNHC})]^-$ (NHC = IMes, **10**; IPr, **11**) and $[\text{Fe}_3(\text{CO})_{10}(\text{CCH}_3)]^-$ (**12**)

The anionic species **1** and **2** were not stable in chlorinated solvents such as CH_2Cl_2 already at room temperature. Complete decomposition occurred after heating at 50 °C, resulting in the formation of the new species $[\text{Fe}_2(\text{CO})_8(\text{AuNHC})]^-$ (NHC = IMes, **10**; IPr, **11**). Formation of **10** and **11** required the formal oxidation of iron from -2, as present in **1** and **2**, to -1, as found in the final products. Since this reaction did not occur in non-chlorinated solvents even after heating for several hours, we could rule out that adventitious oxygen was the oxidizing species. Thus, the oxidant should be CH_2Cl_2 itself.²⁷ Unfortunately, all attempts to identify the products of the reduction of CH_2Cl_2 by GC-MS analyses failed. Therefore, it was not possible to deduce the mechanism of the reaction.

This item was downloaded from IRIS Università di Bologna (<https://cris.unibo.it/>)

When citing, please refer to the published version.

Compounds **10** and **11** were characterized by means of IR and multinuclear NMR spectroscopy, and the molecular structure of **11** crystallographically determined as its [NEt₄][**11**] \cdot 1.5toluene salt (Figure 1). The molecular structure of **11** may be viewed as the result of the addition of a [AuIPr]⁺ fragment to [Fe₂(CO)₈]²⁻. It displayed six terminal and two edge bridging carbonyl ligands, as previously found in the PPh₃-derivative [Fe₂(CO)₈(AuPPh₃)]⁻.²⁸ Conversely, the related copper species [Fe₂(CO)₈(CuPCy₃)]⁻²⁹ displayed only terminal carbonyls. **11** displayed also some short sub-van der Waals Au \cdots C(O) contacts. The structure of **11** was an interesting addition to the limited number of compounds with the Fe₂(CO)₆(μ -CO)₂ unit.^{30,31} The Fe-Fe bond distance of such compounds spanned a very large range [2.39-2.62 Å]. In the case of **11**, the Fe-Fe distance [2.573(4) Å] was in the middle between Fe₂(CO)₉ [2.52 Å]³² and [Fe₂(CO)₈(AuPPh₃)]⁻ [2.605 Å].²⁸

The ¹H and ¹³C{¹H} NMR spectra of **11** (Figures S1 and S2 in Supporting Information) displayed all the expected resonances due to the IPr group. Conversely, in the carbonyl region of the ¹³C{¹H} NMR spectra recorded at 298 and 273 K, only a single sharp resonance at 230.5 ppm was detected. Coalescence was, then, observed at 213 K (Figure S3 in Supporting Information), suggesting the presence of a fluxional behaviour that made the eight CO ligands equivalent at higher temperatures. The structures of **10** and **11** were also optimized by means of DFT calculations. The root-mean-square deviation (RMSD) between the experimental and computed structures of the anion of **11** was quite low (0.311 Å) and the value decreased to 0.183 Å by removing the substituents on the nitrogen atoms from the comparison. The computed structure of **10** strongly resembled that of **11** (Figure S17 in Supporting Information), with negligible variations of bond lengths and angles. This indicated scarce influence of the different substituents on the NHC ligands.

This item was downloaded from IRIS Università di Bologna (<https://cris.unibo.it/>)

When citing, please refer to the published version.

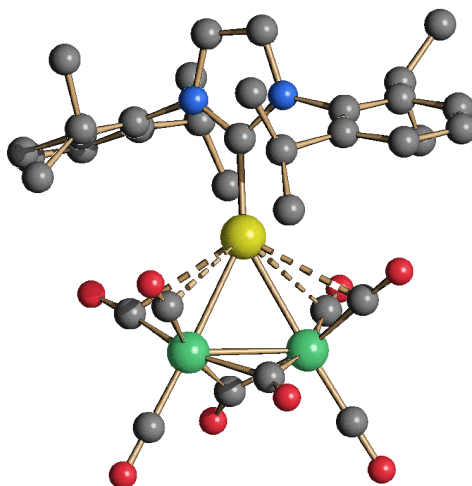


Figure 1. Molecular structure of **11**. Au-C(O) contacts [2.830(19)-2.977(19) Å] were represented as fragmented lines. Hydrogen atoms were omitted for clarity (green Fe; yellow Au; blue N; red O; grey C). Selected bond lengths (Å): Fe-Fe 2.573(4); Fe-Au 2.665(3) and 2.677(3); Au-C_{carbene} 2.013(18); Fe-C(O)_{bridge} 1.90(2)-1.969(18); Fe-C(O)_{terminal} 1.73(2)-1.83(3).

Besides **11** which was the major product, a few crystals of [NEt₄][Fe₃(CO)₁₀(CCH₃)] were isolated as side products of the thermal decomposition of **2** in CH₂Cl₂, and their nature completely revealed by means of X-ray crystallography. These crystals contained the μ₃-ethylidyne cluster [Fe₃(CO)₁₀(CCH₃)]⁻ (**12**) (Figure 2), whose synthesis was previously reported, whereas its structure, at the best of our knowledge, was not described before.³³ The molecular structure of **12** was composed of a triangular Fe₃ core, bonded to nine terminal CO ligands (three per each Fe-atom), one μ₃-ethylidyne and one μ₃-CO. The μ₃-ethylidyne ligand was previously found on related tri-iron carbonyl clusters, such as Fe₃(CO)₈(Cp)(CCH₃),³⁴ H₃Fe₃(CO)₉(CCH₃),³⁵ Fe₃(CO)₉(COCH₃)(CCH₃)³⁶ and Fe₃(CO)₁₀(CuPPh₃)(CCH₃),³⁷ as well as the tetra-iron cluster [Fe₄(CO)₁₂(CCH₃)]⁻.³⁸ It is noteworthy that the closely related Fe₃(CO)₁₀(CuPPh₃)(CCH₃),³⁷ that formally arose from the addition of a [CuPPh₃]⁺ fragment to **12**, displayed nine terminal and one edge bridging μ-CO ligand, instead of a face bridging μ₃-CO. A similar stereochemistry of the carbonyl ligands was found in the μ₃-methylidyne cluster [Fe₃(CO)₁₀(CH)]⁻.³⁹ The bonding parameters of **12** (see caption of Figure 2) were similar to those previously reported for related clusters.³⁴⁻³⁸ The μ₃-CO [Fe-C(O)_{bridging} 2.015(2)-2.077(2) Å] and μ₃-CCH₃ ligands [Fe-C_{ethylidyne} 1.940(2)-1.960(2) Å] were

This item was downloaded from IRIS Università di Bologna (<https://cris.unibo.it/>)

When citing, please refer to the published version.

symmetrically bonded to the Fe₃-triangle and the C-C_{ethynylidene} distance [1.497(3) Å] was as expected for a single bond.

12 was previously synthesized from the reaction of [HFe₃(CO)₁₁]⁻ with acetylene.³³ The mechanism for the formation of **12** as side product along the thermal decomposition of **2**, that afforded **11** as major product, was not clear. It probably involved the oxidation of **2** by means of CH₂Cl₂ as described above followed by removal of the AuIPr fragment and rearrangement of the cluster core. Unfortunately, due to the very low yields, it was not possible to further elucidate the mechanism.

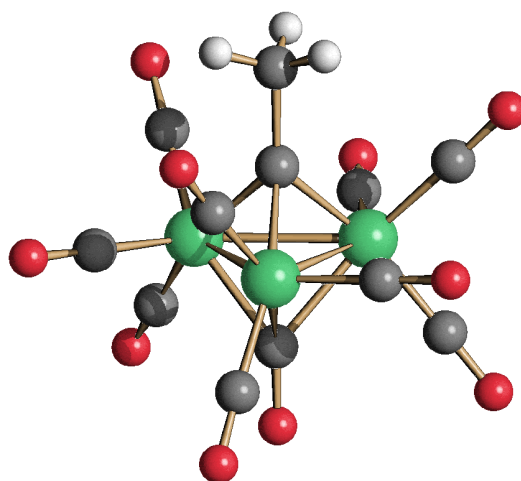


Figure 2. Molecular structure of **12** (green Fe; red O; grey C; white, H). Selected bond lengths (Å): Fe-Fe 2.5285(5)-2.5458(5); Fe-C_{ethynylidene} 1.940(2)-1.960(2); Fe-C(O)_{bridging} 2.015(2)-2.077(2); Fe-C(O)_{terminal} 1.766(3)-1.811(3); C-C_{ethynylidene} 1.497(3).

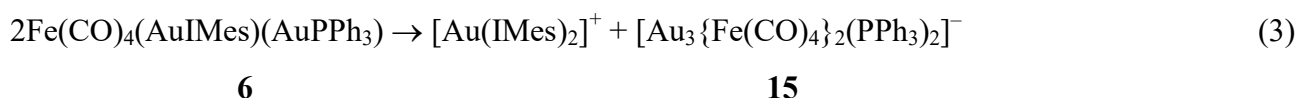
2.2 Syntheses and characterization of [Au₃{Fe(CO)₄}₂(PPh₃)₂]⁻ (**15**)

Complex **6**, that contained mixed IMes/PPh₃ ligands, was not very stable in polar solvents already at room temperature.⁴ Indeed, its ³¹P {¹H} NMR spectrum in CD₃COCD₃ solution displayed a major resonance at δ_p 40.8 ppm attributable to **6**, accompanied by minor resonances at 40.1 ppm and 38.5 ppm (Figures S8 and S9 in Supporting Information). These resonances corresponded to Fe(CO)₄(AuPPh₃)₂ (**14**) and a new species **15**, respectively. The former was a by-product of the synthesis of **6** as previously reported,⁴ whereas the formation of **15** arose from partial decomposition (ionization) of **6**. Indeed, after heating this mixture in CH₃CN at 80 °C for 3 h, the resonance at δ_p 40.8 ppm considerably decreased, whereas the resonance at δ_p 38.5 ppm became the major one (Figure S9). This indicated an almost complete conversion of **6** into **15**. This new

This item was downloaded from IRIS Università di Bologna (<https://cris.unibo.it/>)

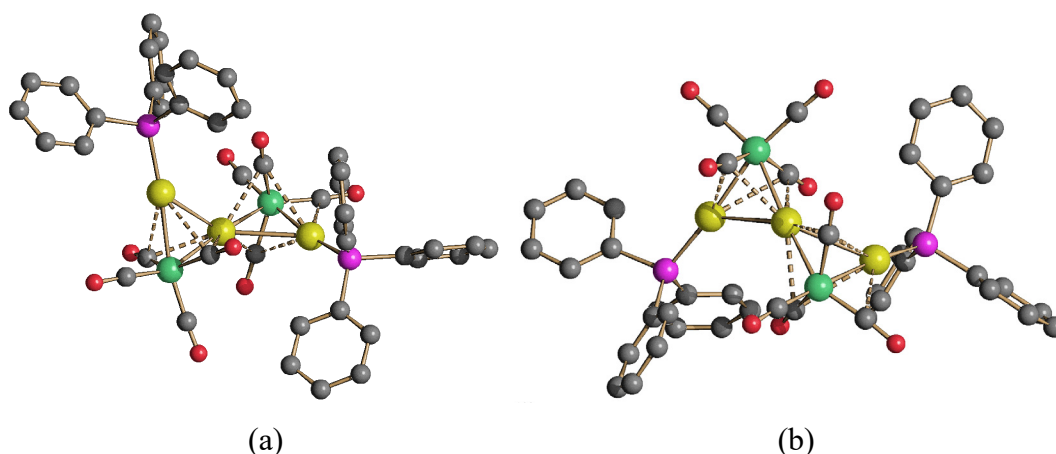
When citing, please refer to the published version.

compound was completely characterized by means of IR, ^1H , $^{13}\text{C}\{^1\text{H}\}$ and $^{31}\text{P}\{^1\text{H}\}$ NMR spectroscopy (Figures S10, S11 and S12 in Supporting Information), and its structure was determined by single crystal X-ray diffraction as its $[\text{Au}(\text{IMes})_2][\mathbf{15}] \cdot 0.67\text{CH}_2\text{Cl}_2$ salt (Figures 3 and 4, and Table S1). The latter was composed of $[\text{Au}(\text{IMes})_2]^+$ cations and $[\text{Au}_3\{\text{Fe}(\text{CO})_4\}_2(\text{PPh}_3)_2]^-$ anions (**15**), in accord to equation 3.



Within the crystals of $[\text{Au}(\text{IMes})_2][\mathbf{15}] \cdot 0.67\text{CH}_2\text{Cl}_2$, two isomers of the anion **15** were present in a 2:1 ratio (referred as isomers **15a** and **15b**, respectively). Both isomers were composed of an Au_3 core bonded to two $\mu\text{-Fe}(\text{CO})_4$ units and two terminal PPh_3 ligands. The Au_3 core of **15a** displayed a V-shaped geometry [$\angle\text{Au-Au-Au } 132.00(4)^\circ$], whereas it adopted a linear arrangement in **15b** with the central Au atom located on an inversion center [$\angle\text{Au-Au-Au } 180.00(10)^\circ$]. The structure of the isomer **15b** was similar to that previously reported for **13**.³ Both isomers displayed two aurophilic $\text{Au}\cdots\text{Au}$ contacts [2.9353(13) and 2.8855(14) Å for **15a**; 2.9177(14) and 2.9177(14) Å for **15b**] as well as sub-van der Waals $\text{Au}\cdots\text{C}(\text{O})$ contacts [2.34(6)-2.87(8) Å for **15a**; 2.56(3)-2.89(3) Å for **15b**].

The presence in the solid state of two isomers of **15** prompted a variable temperature $^{31}\text{P}\{^1\text{H}\}$ NMR investigation. Unfortunately, a single resonance was observed at all the temperatures examined (193-298 K) suggesting a fast exchange between **15a** and **15b** in solution.



This item was downloaded from IRIS Università di Bologna (<https://cris.unibo.it/>)

When citing, please refer to the published version.

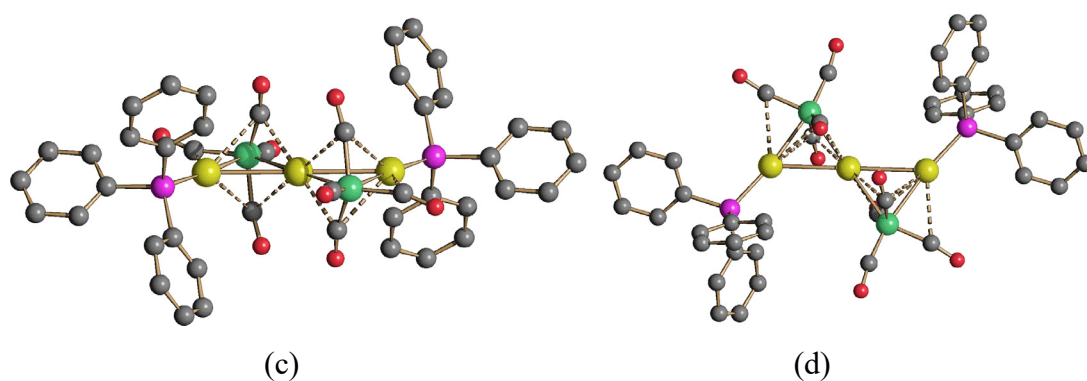


Figure 3. Molecular structures of the two isomers of **15**. The two isomers were present within the crystal in the ratio **15a:15b** = 2:1. Two views of isomer **15a** are reported in (a) and (b), two views of isomer **15b** are reported in (c) and (d). Au-C(O) contacts [2.34(6)-2.87(8)Å for **15a**; 2.56(3)-2.89(3) Å for **15b**] were represented as fragmented lines. Hydrogen atoms have been omitted for clarity (green Fe; yellow Au; purple P; blue N; red O; grey C)

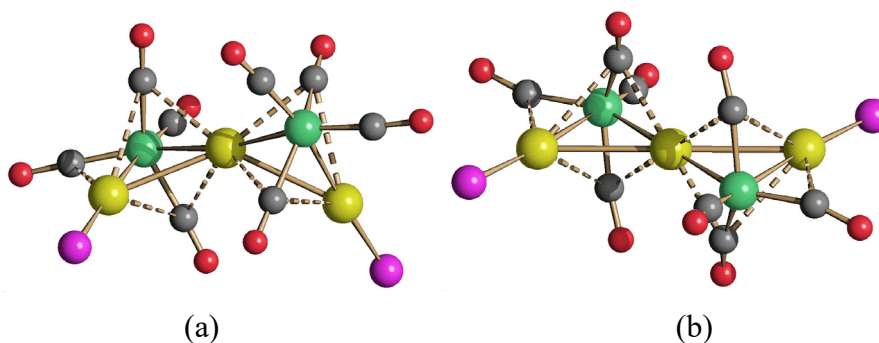


Figure 4. The $\text{Au}_3\text{Fe}_2(\text{CO})_8\text{P}_2$ cores of (a) **15a** and (b) **15b** (green Fe; yellow Au; purple P; red O; grey C).

The structures of **15a** and **15b** were also optimized by means of DFT calculations. The RMSD of the computed $[\text{Fe}_2\text{Au}_3]$ cores with respect to the experimental data were 0.129 and 0.064 Å respectively for **15a** and **15b**. The deviations were mainly attributable to a slight overestimation of the Au–Au distances, caused by the known weakness of DFT methods in predicting dispersion interactions such as the aurophilic one.⁴⁰ Despite this limit, the computed energy difference between the two isomers was 0.9 kcal mol⁻¹, **15a** resulting slightly more stable than **15b**, in agreement with the fast exchange observed. In both the clusters, no (3,-1) bond critical point (b.c.p.) for Au–Au interactions was found, being the gradient norm of electron density higher than zero along the Au–Au bonds (minimum gradient values were 0.005 and 0.004 a.u. for **15a** and **15b**, respectively).

This item was downloaded from IRIS Università di Bologna (<https://cris.unibo.it/>)

When citing, please refer to the published version.

This result, that suggested a delocalized dispersion interaction, was in line with the data previously reported for **8**.⁷ (3,-1) b.c.p. were instead found for the Fe-Au bonds, and relevant data were collected in Table S2 and compared with those obtained for compounds **10** and **11**. All Fe-Au b.c.p. were characterized by negative energy density (E) values, while the Laplacian of electron density ($\nabla^2 \rho$) was positive, in agreement with Bianchi's definition of M-M bonds.⁴¹ ρ and V values of **15a** and **15b** were closely comparable, and the bonds with terminal Au atoms were stronger than those with the central Au. The data collected in Table S2 indicated that the different binding mode of Au in **10** and **11** caused a slightly lowering of the Fe-Au bond strength. For what concerns the charge distribution, the three Au atoms in **15a** and **15b** had very similar Hirshfeld partial charge, in the range 0.060 – 0.064 a.u. for **15a** and 0.057 – 0.065 a.u. for **15b**, as expected on considering the formal homogeneity of the oxidation states.

2.3 Syntheses and characterization of $[\text{Au}_{16}\text{S}\{\text{Fe}(\text{CO})_4\}_4(\text{IPr})_4]^{\text{n}+}$ (**17**)

4 was recovered almost intact also after heating in dmsO at 140 °C for 5 h. It started to show a partial decomposition only after prolonged heating above 150 °C in dmsO. Among the decomposition products, it was possible to isolate a few crystals of $[\text{NEt}_4]_2[\text{Fe}_3\text{S}(\text{CO})_9]$ ($[\text{NEt}_4][\mathbf{9}]$), $[\text{Au}(\text{IPr})_2][\text{HFe}(\text{CO})_4]$ ($[\text{Au}(\text{IPr})_2][\mathbf{16}]$) and $[\text{Au}_{16}\text{S}\{\text{Fe}(\text{CO})_4\}_4(\text{IPr})_4][\text{BF}_4]_n \cdot \text{solv}$ ($[\mathbf{17}][\text{BF}_4]_n \cdot \text{solv}$). The presence of $[\text{BF}_4]^-$ anions in the latter salt was due to the use of $[\text{NEt}_4][\text{BF}_4]$ during workup of the reaction mixture.

The anions **9** and **16** were previously reported and,^{26,42} therefore, their structures will not be discussed any further. Their crystal data were deposited within the Cambridge Crystallographic Datacenter and a representation of the molecular structure of **9** was included as Figure S16 in the Supporting Information.

Formation of **9** was rather interesting since it suggested that S-atoms were somehow generated from dmsO after the prolonged thermal treatment of **4**. This was in keeping with the formation of the new species **17**, which contained an interstitial sulfur atom. Compound **17** was formed only in trace amounts and because of this, only very few small crystals were grown. This allowed the complete determination of the molecular structure of the cluster molecule (Figure 5 and Table S3), which occupied 78% of the unit cell volume. The remaining 22% of the volume of the unit cell was likely to be occupied by cations/anions and/or solvent molecules (Figure S17 in Supporting Information), whose nature was not determined.

This item was downloaded from IRIS Università di Bologna (<https://cris.unibo.it/>)

When citing, please refer to the published version.

Despite the fact that **17** was obtained in low yields, it was possible to characterize it also by means of multinuclear NMR techniques. ^1H and $^{13}\text{C}\{^1\text{H}\}$ NMR analyses were in agreement with the presence of CO and IPr ligands (Figures S13 and S14 in Supporting Information). More interestingly, the ^{19}F NMR spectrum of **17** (Figure S15 in Supporting Information) displayed the typical resonance of the $[\text{BF}_4]^-$ anion. Therefore, **17** was better formulated as a cationic species and because of this, its crystals were referred as $[\mathbf{17}][\text{BF}_4]_n \cdot \text{solv}$.

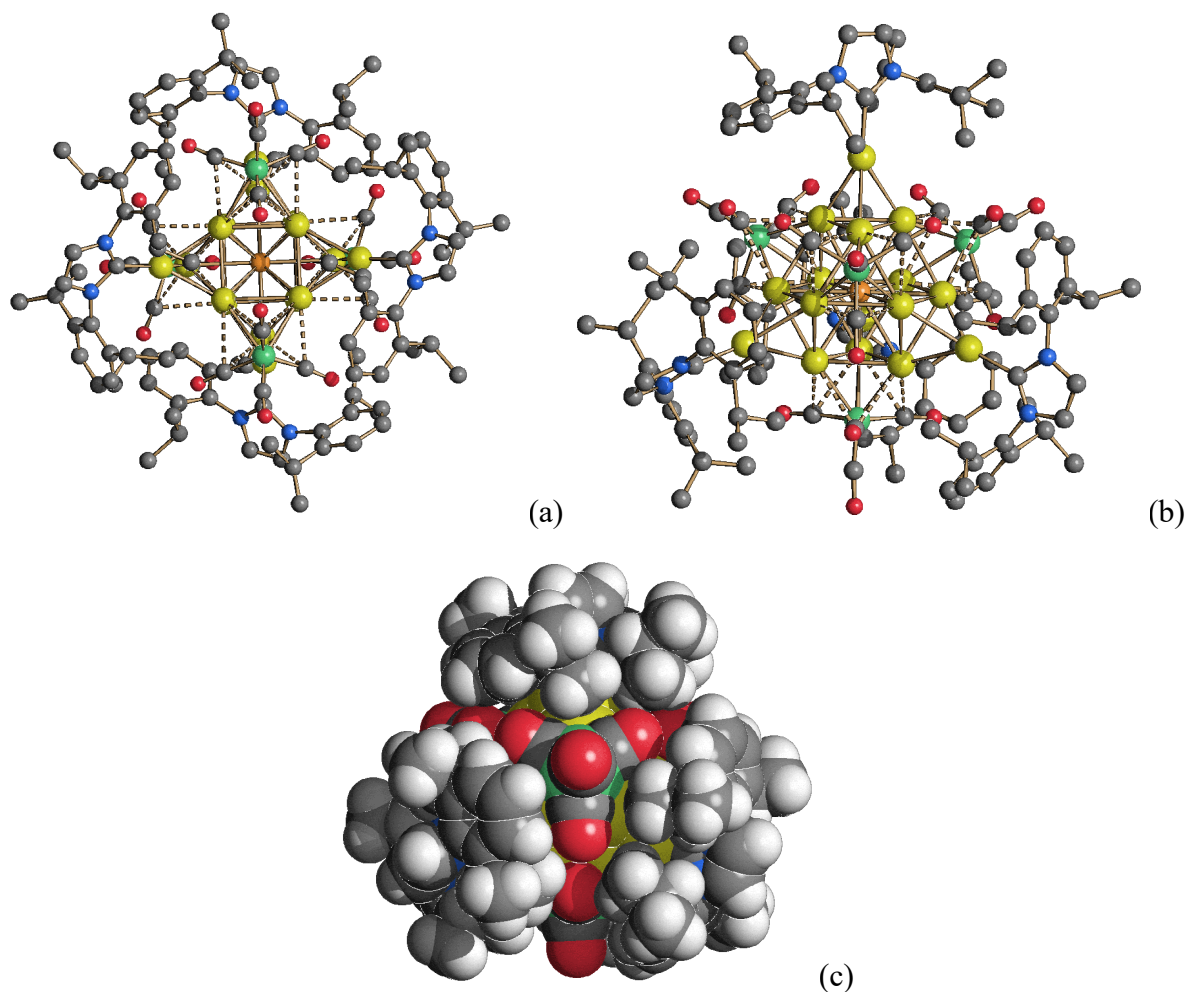


Figure 5. Molecular structure of **17**. Two different views (a,b) as well as the space filling model (c) were reported. Au-C(O) contacts [2.636(4)-2.723(4) Å] were represented as fragmented lines. Hydrogen atoms have been included only in the space filling model (green Fe; yellow Au; orange S; blue N; red O; grey C; white, H).

This item was downloaded from IRIS Università di Bologna (<https://cris.unibo.it/>)

When citing, please refer to the published version.

17 consisted of a Au₁₂-cubeoctahedron centered by a μ₁₂-S atom, whose surface was decorated by four μ₃-Fe(CO)₄ and four μ₃-AuIPr fragments with a pseudo-T_d symmetry (Figure 6). A related structure, where a μ₁₂-S atom was encapsulated within a Cu₁₂-cubeoctahedral cage, was recently reported for the neutral [Cu₁₂(μ₁₂-S)(S₂CNⁿBu₂)₆(C≡CPh)₄] cluster.⁴³ As in the case of [Cu₁₂(μ₁₂-S)(S₂CNⁿBu₂)₆(C≡CPh)₄], the Au-S distances [2.7641(13)-2.7995(16) Å, average 2.777(3) Å] of **17** were rather elongated in view of the high coordination number of the interstitial μ₁₂-S atom. For comparison, the sums of the covalent and van der Waals radii of Au and S were 2.38 and 3.46 Å, respectively.⁴⁴ Prior of the isolation of **17**, the highest coordination number observed for S with Au was four, and the corresponding Au-S distances were considerably shorter [2.30-2.42 Å].^{45,46}

The tangential Au-Au contacts [2.702(2)-2.874(2) Å, average 2.753(6) Å] were more dispersed compared to the more localised Au-Au contacts involving the μ₃-AuIPr fragments [2.724(2)-2.733(2) Å, average 2.728(3) Å]. Similarly, the Au-Fe distances [2.625(5)-2.650(5) Å, average 2.636(9) Å] displayed by **17** that presented μ₃-Fe(CO)₄ groups were significantly longer than those found in clusters containing μ₂-Fe(CO)₄ fragments such as **15** [2.529(3)-2.601(11) Å, average 2.564(8) Å].

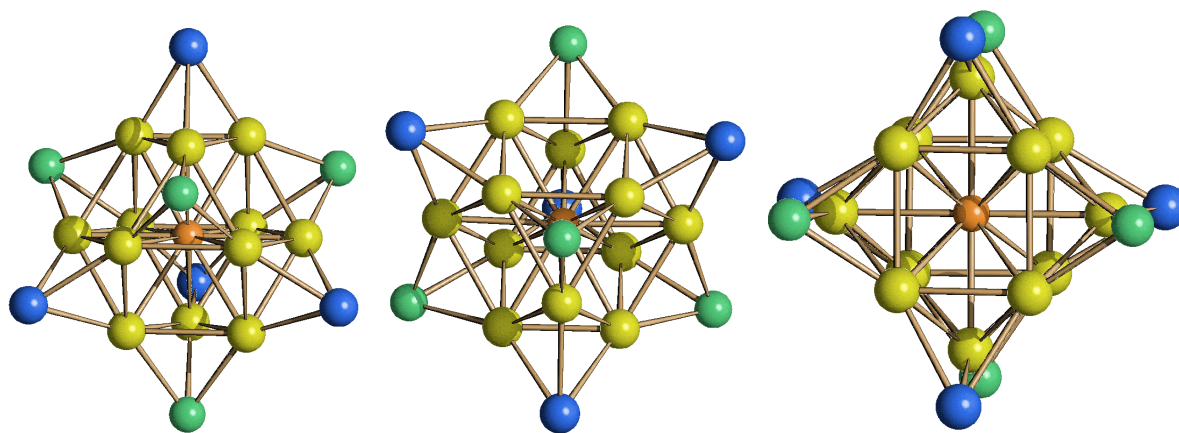


Figure 6. Three different views of the Au₁₆S core of **17** (green Fe; yellow Au atoms of the Au₁₂ cubeoctahedron; blue Au atoms of the μ₃-AuIPr fragments; orange S).

Molecular gold nanoclusters stabilized by ligands were extensively studied in the recent years.¹¹⁻²² Au₁₃ and Au₁₂M cages often adopted icosahedral structures, but also a few clusters displaying a cubeoctahedral structure were reported.¹⁵ This point was also computationally

This item was downloaded from IRIS Università di Bologna (<https://cris.unibo.it/>)

When citing, please refer to the published version.

investigated showing that, depending on the central atom, Au_{12}M clusters could adopt I_h (icosahedron) or O_h (cuboctahedron) symmetry.⁴⁷

DFT calculations were carried out on models of compound **17**. The substituents on the nitrogen atoms of the NHC ligands were replaced by methyl groups to reduce the computational effort. The coordinates of the other atoms were obtained from X-ray data. The singlet multiplicity was always maintained, and the charge was varied from 2+ to 6+. The most stable electronic structure resulted to be the most reduced one, that is 2+. The 4+ and 6+ cations were less stable by 0.9 and 2.2 a.u., respectively. For this reason, the formula $[\text{Au}_{16}\text{S}\{\text{Fe}(\text{CO})_4\}_4(\text{IPr})_4]^{2+}$ was proposed. The computed energy gap between frontier orbitals in the model compound was quite high, 3.9 eV.

The approximate T_d symmetry was confirmed by all the population analyses, and the four C_3 axes were reported in Figure 7 for clarity. The compound can be thought as composed of four $[\text{FeAu}_3]$ tetrahedra, each one forming three bonds with the central sulphur. One of the $[\text{FeAu}_3]$ tetrahedra and its bonds with S were highlighted in red in Figure 7. The $[\text{FeAu}_3]$ tetrahedra were interconnected by Au-Au bonds, and each $[\text{AuNHC}]$ fragment (NHC = 1,3-dimethylimidazol-2-ylidene) was bonded to three Au atoms belonging to different $[\text{FeAu}_3]$ tetrahedra, with the formation of $[\text{Au}_4]$ tetrahedra, one of them highlighted in Figure 7. The bonds involving the Au centres can be therefore grouped into six types, as depicted in Figure 7: (a) Au-S; (b) Au-Fe; (c) Au-Au in $[\text{FeAu}_3]$; (d) Au-Au in $[\text{Au}_4]$, between iron-bonded centres; (e) Au-Au in $[\text{Au}_4]$ involving the $[\text{AuNHC}]$ fragment; (f) Au-NHC. Average values concerning the (3,-1) b.c.p were collected in Table S4. It is worth noting that the AIM analysis was unable to find (3,-1) b.c.p. associated to Au-CO interactions.

As for the previously discussed compounds, all the b.c.p. considered in Table S4 were characterized by negative E and positive $\nabla^2\rho$ values, in agreement with the definition of M-M and dative bonds.⁴¹ The Au-Au bonds in the $[\text{Au}_4]$ tetrahedra had similar ρ and V values at b.c.p., this indicating comparable strength. The Au-Au interactions in the $[\text{FeAu}_3]$ fragments were comparatively slightly weaker. On considering the Au-S, Au-Fe and Au-Au bonds, the V values fell in a quite limited range, comprised between -0.034 and -0.062 a.u., while the average V value related to the Au-NHC b.c.p. was meaningfully more negative, -0.193 a.u. The picture coming from the AIM analysis was that the Au, S and Fe atoms in **17** formed a network of bonds having roughly comparable strength.

This item was downloaded from IRIS Università di Bologna (<https://cris.unibo.it/>)

When citing, please refer to the published version.

The partial charges on the Au atoms obtained from the Hirshfeld population analysis were comprised between 0.059 and 0.126 a.u. The less positive values were related to the NHC-bonded Au atoms, probably because of the donation from the ligands. The maximum charge variation among the other Au centres was 0.03 a.u., this supporting a homogeneous distribution of electron density. Quite interestingly, also the Hirshfeld charge on sulphur was slightly positive (0.045 a.u.). Therefore, AIM and Hirshfeld data suggested that the behaviour of the central sulphur was roughly comparable to that of the surrounding Au atoms. Finally, as expected the Hirshfeld charge on Fe atoms was negative, -0.176 a.u.

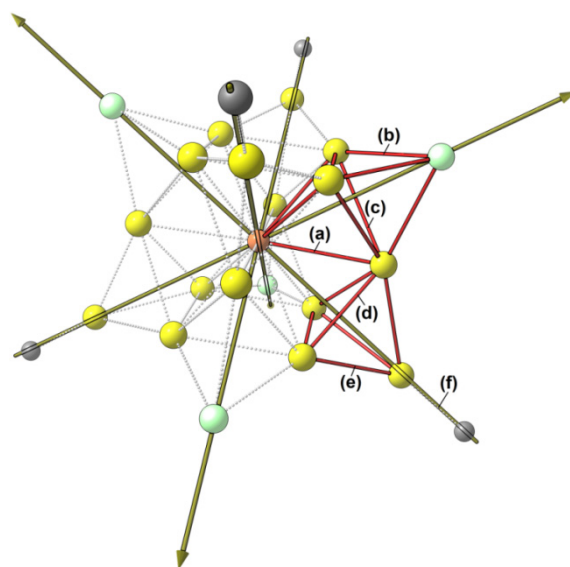


Figure 7. Structure of **17** with highlighted one [FeAu₃] and one [Au₄] tetrahedron. The CO ligands were removed for clarity. Only the donor atoms of the NHC ligands were depicted. The four C₃ axes were shown. Different types of bonds involving the Au centres were labelled. Colour map: Au, yellow; S, orange; Fe, green; C, grey.

The electron count of **17** was based on the following assumptions. The μ_3 -AuIPr fragments were considered to contribute one electron each, being isolobal to μ_3 -H. The μ_3 -Fe(CO)₄ groups were usually described in the literature as four electron donors.⁴⁸ The interstitial μ_6 -S atom was considered to contribute with all its six valence electrons. Therefore, if **17** was a dication, as inferred from DFT calculations, it should possess 156 [11×12 (Au) + 6×1 (μ_6 -S) + 4×1 (μ_3 -AuIPr) + 4×4 (μ_3 -Fe(CO)₄) - 2 (charge +2)] cluster valence electrons (CVE). The expected CVEs depended of the model adopted. According to the EAN (Effective Atomic Number) rule, a cubeoctahedron should have 168 CVE. PSEPT (Polyhedral Skeletal Electron Pair Theory) predicted

This item was downloaded from IRIS Università di Bologna (<https://cris.unibo.it/>)

When citing, please refer to the published version.

170 CVE by interpreting a cubeoctahedron as a four-connected polyhedron. Conversely, assuming that radial bonding predominates, on the basis of Mingos Rules a cubeoctahedron should have 162 CVE.^{48,49} In this respect, **17** appeared to be electron poor, as often happened for gold clusters.⁴⁹

3. Conclusions

Low nuclearity Fe-Au compounds **1-7** were thermally decomposed to high nuclearity species. The obtained Fe-Au products could be grouped within the following categories:

- 1) products **8**, **13** and **15** were the result of ionization and rearrangement of the starting species. Thus, they retained the original oxidation states of the metals, that is Au(+1) and Fe(-2).
- 2) **10** and **11** resulted from oxidation of iron from -2 to -1, whereas gold retained the original +1 oxidation state.
- 3) the unique species **17** (even if obtained in very low yields) formally contained Fe(-2) whereas the oxidation state of Au was comprised between 0 and +1. This assignment was based on the assumption that, as usually found in Au-Fe carbonyl clusters,^{1,3-8} the Fe(CO)₄ fragments retained the original dianionic nature.

All the heterometallic clusters reported contained strong Fe-CO, Fe-Au, Au-P and Au-NHC bonds as well as weak Au...Au interactions. AIM analyses and DFT studies pointed out that the Au...Au interactions in such heterometallic clusters were mainly dispersion-driven. In addition, the different behavior of IMes and IPr derivatives was essentially due to steric effects, since no appreciable electronic difference is evidenced by population analyses based on DFT calculations, as previously reported.⁴

IPr-containing species were in general more stable than IMes-ones. In all cases, even by heating **1-7** up to 160 °C the formation of carbido clusters was not observed. This was probably due to the presence of the AuNHC fragments, since in their absence, anions of iron carbonyls afforded Fe₅ and Fe₆ carbido clusters.^{50,51}

4. Experimental

4.1 General experimental procedures

All reactions and sample manipulations were carried out using standard Schlenk techniques under nitrogen and in dried solvents. All the reagents were commercial products (Aldrich) of the highest purity available and used as received, except **1-7** which were prepared according to the literature.^{3,4}

This item was downloaded from IRIS Università di Bologna (<https://cris.unibo.it/>)

When citing, please refer to the published version.

Analyses of C, H and N were obtained with a Thermo Quest Flash EA 1112NC instrument. IR spectra were recorded on a Perkin Elmer Spectrum One interferometer in CaF₂ cells. Structure drawings have been performed with SCHAKAL99.⁵²

4.2 Thermal decomposition of [NEt₄][Fe(CO)₄(AuNHC)] (NHC = IMes, **1**; IPr, **2**) in non-chlorinated solvents.

A solution of [NEt₄][**1**] (0.530 g, 0.663 mmol) in dmsO (10 mL) was heated at 130 °C for 3 h and the reaction monitored by IR spectroscopy. Then, a saturated solution of [NEt₄]Br in H₂O (40 mL) was added up to complete precipitation. The resulting solid was recovered by filtration, washed with H₂O (3 × 15 mL), toluene (3 × 15 mL), and extracted with acetone (15 mL). A microcrystalline powder of [NEt₄]₃[**8**] was obtained after removal of the solvent under reduced pressure (yield 0.134 g, 41 % based on Fe, 41 % based on Au). The compound was identified by comparison of its IR data with those reported in the literature.⁷

Decomposition of [NEt₄][**2**] to produce **8** occurred at 150 °C in dmsO. By further increasing the temperature up to 160-170 °C, a complex mixture of decomposition products was formed, among which **9** was the major species detected by IR spectroscopy.

4.3 Synthesis of [Fe₂(CO)₈(AuNHC)]⁻ (NHC = IMes, **10**; IPr, **11**).

A solution of [NEt₄][**2**] (0.530 g, 0.600 mmol) in CH₂Cl₂ (20 mL) was heated at 40 °C for 4 h and the reaction monitored by IR spectroscopy. Then, the solvent was removed under reduced pressure and the residue washed with H₂O (3 × 15 mL), and extracted with toluene (10 mL). Crystals of [NEt₄][**11**].1.5toluene suitable for X-ray crystallography were obtained by slow diffusion of n-pentane (25 mL) on the toluene solution (yield 0.207 g, 58 % based on Fe, 29 % based on Au).

A few crystals of [NEt₄][**12**] were isolated as side products of the thermal decomposition of **2** in CH₂Cl₂, and their nature completely revealed by means of X-ray crystallography.

[NEt₄][**11**].1.5toluene - C_{53.5}H₆₈AuFe₂N₃O₈ (1189.77): calcd. (%): C 59.98, H 5.76, N 3.53; found: C 60.12, H 5.38, N 3.21. IR (nujol, 293 K) ν_{CO}: 2004(w), 1956(s), 1923(ms), 1895(vs), 1880(sh) cm⁻¹. IR (dmsO, 293 K) ν_{CO}: 2004(w), 1958(s), 1913(sh), 1900(vs), 1728(ms) cm⁻¹. IR (CH₃CN, 293 K) ν_{CO}: 2006(w), 1960(s), 1903(vs), 1727(ms) cm⁻¹. IR (acetone, 293 K) ν_{CO}: 2004(w), 1958(s), 1912(sh), 1902(vs) cm⁻¹. IR (toluene, 293 K) ν_{CO}: 2005(w), 1963(s), 1900(vs), 1721(m) cm⁻¹. IR (CH₂Cl₂, 293 K) ν_{CO}: 2007(w), 1961(s), 1905(vs), 1715(ms) cm⁻¹. IR (thf, 293 K) ν_{CO}:

This item was downloaded from IRIS Università di Bologna (<https://cris.unibo.it/>)

When citing, please refer to the published version.

2002(w), 1959(s), 1904(vs), 1720(m) cm^{-1} . ^1H NMR (CD_3COCD_3 , 298 K): δ 7.50-7.24 (m, 8H, $\text{CH}_{\text{Ar}} + \text{CH}_{\text{imid}}$), 3.44 (q, $^2J_{\text{HH}} = 6.2$ Hz, 8H, NCH_2CH_3), 2.95 (sept, $^2J_{\text{HH}} = 6.8$ Hz, 4H, $\text{CH}(\text{CH}_3)_2$), 1.36 (d, $^2J_{\text{HH}} = 6.8$ Hz, 12H, $\text{CH}(\text{CH}_3)_2$), 1.35 (t, $^2J_{\text{HH}} = 6.2$ Hz, 12H, NCH_2CH_3), 1.15 (d, $^2J_{\text{HH}} = 6.8$ Hz, 12H, $\text{CH}(\text{CH}_3)_2$). $^{13}\text{C}\{^1\text{H}\}$ NMR (CD_3COCD_3 , 298 K): δ 231.5 (CO), 200.4 (C-Au), 145.4, 135.9, 129.4, 123.7, 123.3 (C_{Ar} and CH_{imid}), 51.9 (NCH_2CH_3), 28.2 ($\text{CH}(\text{CH}_3)_2$), 23.9, 23.3 ($\text{CH}(\text{CH}_3)_2$), 6.7 (NCH_2CH_3).

The thermal decomposition of **1** under the same experimental conditions described above afforded $[\text{Fe}_2(\text{CO})_8(\text{AuIMes})]^-$ (**10**). IR (CH_2Cl_2 , 293 K) ν_{CO} : 2000(w), 1959(s), 1899(vs), 1712(ms) cm^{-1} .

4.4 Synthesis of $[\text{NBu}_4][\text{Au}_3\text{Fe}_2(\text{CO})_8(\text{IMes})_2] \cdot \text{CH}_3\text{COCH}_3$ ($[\text{NBu}_4][\mathbf{13}] \cdot \text{CH}_3\text{COCH}_3$)

A large excess of $[\text{NBu}_4][\text{BF}_4]$ was added as a solid to a solution of **3** (0.190 g, 0.531 mmol) in dmf (20 mL), and the mixture stirred at 100°C for 1 h. Then, the orange solution was cooled down to room temperature and H_2O (60 mL) was added until complete precipitation occurred. The solid was recovered by filtration, washed with H_2O (40 mL) and extracted in acetone (10 mL). Needle-like pale yellow crystals of $[\text{NBu}_4][\mathbf{13}] \cdot \text{CH}_3\text{COCH}_3$ suitable for X-ray analyses were obtained by slow diffusion of n-hexane (30 mL) on the acetone solution (yield 122 g, 25 % based on Fe).³

$\text{C}_{69}\text{H}_{90}\text{Au}_3\text{Fe}_2\text{N}_5\text{O}_9$ (1836.06): calcd. (%): C 45.11, H 4.94, N 3.81, Fe 6.09, Au 32.19; found: C 45.41, H 5.12, N 3.62, Fe 6.31, Au 31.85. IR (nujol, 293 K) ν_{CO} : 1948(vs), 1877(sh), 1867(s), 1836(sh), 1712(m) cm^{-1} . IR (acetone, 293 K) ν_{CO} : 1968(sh), 1947(m), 1924(m), 1872(s) cm^{-1} . ^1H NMR (CD_2Cl_2 , 298 K): δ 7.12 (s, 8H, CH_{imid}), 6.94 (s, 16H, CH_{Ar}), 3.20 (br, 8H, $\text{NCH}_2\text{CH}_2\text{CH}_2\text{CH}_3$), 2.47 (s, 24H, CH_3), 1.74 (s, 48H, CH_3), 1.65 (br, 8H, $\text{NCH}_2\text{CH}_2\text{CH}_2\text{CH}_3$), 1.47 (br, 8H, $\text{NCH}_2\text{CH}_2\text{CH}_2\text{CH}_3$), 1.01 (br, 12H, $\text{NCH}_2\text{CH}_2\text{CH}_2\text{CH}_3$). $^{13}\text{C}\{^1\text{H}\}$ NMR (CD_2Cl_2 , 298 K): δ 220.9 (CO), 185.3 (C-Au), 139.4, 134.6, 134.1, 129.0 (C_{Ar}), 122.8 (CH_{imid}), 58.6 ($\text{NCH}_2\text{CH}_2\text{CH}_2\text{CH}_3$), 23.7 ($\text{NCH}_2\text{CH}_2\text{CH}_2\text{CH}_3$), 19.6 ($\text{NCH}_2\text{CH}_2\text{CH}_2\text{CH}_3$), 20.9, 16.9 (CH_3), 13.3 ($\text{NCH}_2\text{CH}_2\text{CH}_2\text{CH}_3$).

4.5 Synthesis of $[\text{NMe}_4]_2[\text{Au}(\text{IMes})_2][\text{Au}_3\{\text{Fe}(\text{CO})_4\}_3]$ ($[\text{NMe}_4]_2[\text{Au}(\text{IMes})_2][\mathbf{8}]$)

A solution of **3** (0.450 g, 0.384 mmol) in dmsO (15 mL) was heated at 130°C for 0.5 h and the reaction monitored by IR spectroscopy. Then, a saturated solution of $[\text{NMe}_4]\text{Cl}$ in H_2O (40 mL) was added up to complete precipitation. The resulting solid was recovered by filtration, washed

This item was downloaded from IRIS Università di Bologna (<https://cris.unibo.it/>)

When citing, please refer to the published version.

with H₂O (3 × 15 mL), toluene (3 × 15 mL), and extracted with acetone (15 mL). Crystals of [NMe₄]₂[Au(IMes)₂][**8**] suitable for X-ray crystallography were obtained by slow diffusion of n-hexane (35 mL) on the acetone solution (yield 0.14 g, 52 % based on Fe, 36 % based on Au).⁷ [NEt₄]₂[Au(IMes)₂][**8**]·CH₃COCH₃ was obtained following a similar procedure and employing [NEt₄]Br instead of [NMe₄]Cl.

[NMe₄]₂[Au(IMes)₂][**8**] - C₆₂H₇₂Au₄Fe₃N₆O₁₂ (2048.67): calcd. (%): C 36.32, H 3.54, N 4.10; found: C 36.14, H 3.71, N 3.89. IR (nujol, 293 K) ν_{CO}: 1970(m), 1932(s), 1843(s) cm⁻¹. IR (dmsO, 293 K) ν_{CO}: 1974(w), 1930(s), 1879(s) cm⁻¹. IR (CH₂Cl₂, 293 K) ν_{CO}: 1975(w), 1929(s), 1877(s) cm⁻¹. IR (CH₃CN, 293 K) ν_{CO}: 1929(s), 1867(s) cm⁻¹. IR (acetone, 293 K) ν_{CO}: 1969(w), 1928(s), 1864(s) cm⁻¹. ¹H NMR (CD₃CN, 298 K): δ 7.25 (s, 4H, CH_{imid}), 6.98 (s, 8H, CH_{Ar}), 3.17 (s, 24H, NMe₄), 2.45 (s, 12H, CH₃), 1.72 (s, 24H, CH₃). ¹³C{¹H} NMR (CD₂Cl₂, 298 K): δ 224.4 (CO), 185.3 (C-Au), 139.7, 135.0, 134.6, 129.2 (C_{Ar}), 123.4 (CH_{imid}), 55.6 (¹J_{CN} = 3.9 Hz, NMe₄), 20.6, 16.7 (CH₃).

4.6 Synthesis of [Au(IMes)₂][Au₃{Fe(CO)₄}₂(PPh₃)₂]·0.67CH₂Cl₂ ([Au(IMes)₂][**15**]·0.67CH₂Cl₂)

A solution of **6** (0.220 g, 0.188 mmol) in CH₃CN (15 mL) was heated at 80 °C for 3 h and the reaction monitored by IR spectroscopy. Then, a saturated solution of [NEt₄]Br in H₂O (40 mL) was added up to complete precipitation. The resulting solid was recovered by filtration, washed with H₂O (3 × 15 mL), toluene (3 × 15 mL), and extracted with CH₂Cl₂ (15 mL). Crystals of [Au(IMes)₂][**15**]·0.67CH₂Cl₂ suitable for X-ray crystallography were obtained by slow diffusion of n-pentane (35 mL) on the CH₂Cl₂ solution (yield 0.110 g, 51 % based on Fe, 51 % based on Au).

C_{86.67}H_{79.33}Au₄Cl_{1.33}Fe₂N₄O₈P₂ (2313.64): calcd. (%): C 44.98, H 3.46, N 2.42; found: C 45.12, H 3.71, N 2.14. IR (nujol, 293 K) ν_{CO}: 1977(w), 1953(s), 1887(s), 1864(sh), 1843(sh) cm⁻¹. IR (CH₃CN, 293 K) ν_{CO}: 1989(w), 1965(m), 1891(s) cm⁻¹. IR (acetone, 293 K) ν_{CO}: 1988(w), 1963(m), 1891(s) cm⁻¹. ¹H NMR (CD₃COCD₃, 298 K): δ 7.85–6.98 (m, 42 H, CH_{Ar}+CH_{imid}+Ph), 2.46 (s, 12H, CH₃), 1.76 (s, 24H, CH₃). ¹³C{¹H} NMR (CD₃COCD₃, 298 K): δ 220.8 (CO), 185.1 (C-Au), 139.3, 134.6, 134.4, 134.2, 130.6, 129.0, 128.9, 128.8, 123.3 (CH_{Ar}+CH_{imid}+Ph), 20.3, 16.4 ppm (CH₃). ³¹P{¹H} NMR (CD₃COCD₃, 298 K): δ 38.5 ppm.

This item was downloaded from IRIS Università di Bologna (<https://cris.unibo.it/>)

When citing, please refer to the published version.

4.7 Thermal decomposition of Fe(CO)₄(AuIPr)₂ (**4**)

4 was very stable in solution even after heating at 130-150 °C in dmsO. The reactions were periodically monitored by IR spectroscopy and, even after 12-24 hours, the main ν_{CO} bands present in the spectra were those attributable to the starting **4**. Then, a saturated solution of [NEt₄][BF₄] in H₂O (40 mL) was added up to complete precipitation. The resulting solid was recovered by filtration, washed with H₂O (3 × 15 mL), toluene (3 × 15 mL), and extracted with solvent of increasing polarity: CH₂Cl₂ (15 mL), thf (15 mL), acetone (15 mL), CH₃CN (15 mL), and dmsO (15 mL). **4** was the main product recovered independently of the experimental conditions. Nonetheless, several attempts of crystallization were made by layering suitable solvents on the above mentioned solutions. Beside crystals of **4**, these attempts resulted in a few crystals of [Au(IPr)₂][**16**], [NEt₄]₂[**9**], and [**17**][BF₄]_n·solv. These were likely to arise from partial decomposition of **4**, that involved also dmsO activation and formation of sulfide ions. The crystals of [Au(IPr)₂][**16**], [NEt₄]₂[**9**], and [**17**][BF₄]_n·solv were separated from the reaction mixtures and analyzed by X-ray crystallography, as well as IR spectroscopy ([NEt₄]₂[**9**], and [**17**][BF₄]_n·solv) and ¹H, ¹⁹F and ¹³C{¹H} NMR spectroscopy ([**17**][BF₄]_n·solv).

[NEt₄]₂[**9**]. IR (nujol, 293 K) ν_{CO} : 1999(m), 1820(s), 1892(s), 1865(m) cm⁻¹. IR (CH₃CN, 293 K) ν_{CO} : 1988(m), 1932(s), 1904(m), 1873(w) cm⁻¹.

[**17**][BF₄]_n·solv. IR (nujol, 293 K) ν_{CO} : 1975(s), 1903(m), 1856(w) cm⁻¹. IR (CH₂Cl₂, 293 K) ν_{CO} : 2039(m), 1974(s), 1883(s), 1863(m) cm⁻¹. IR (thf, 293 K) ν_{CO} : 2037(m), 1975(s), 1899(s), 1885(s), 1867(m) cm⁻¹. IR (acetone, 293 K) ν_{CO} : 2037(m), 1973(s), 1885(s), 1869(m) cm⁻¹. ¹H NMR (CD₃COCD₃, 298 K): δ 7.51 (s, 8H, CH_{imid}), 7.43 (t, ²J_{HH} = 7.7 Hz, 8H, CH_{Ar}), 7.26 (d, ²J_{HH} = 7.7 Hz, 16H, CH_{Ar}), 2.67 (sept, ²J_{HH} = 7.4 Hz, 16H, CH(CH₃)₂), 1.25(d, ²J_{HH} = 7.4 Hz, 48H, CH(CH₃)₂), 1.17 (d, ²J_{HH} = 7.4 Hz, 48H, CH(CH₃)₂). ¹³C{¹H} NMR (CD₃COCD₃, 298 K): δ 222.3 (CO), 199.2 (C-Au), 150.6, 140.2, 135.0, 128.9, 128.1 (C_{Ar} and CH_{imid}), 33.7 (CH(CH₃)₂), 28.9, 28.7 (CH(CH₃)₂). ¹⁹F NMR (CD₃COCD₃, 298 K): δ -151.76, -151.81 ([BF₄]⁻).

4.8 Thermal decomposition of Fe(CO)₄(AuIMes)(AuIPr) (**5**)

A solution of **5** (0.450 g, 0.359 mmol) in dmsO (15 mL) was heated at 130 °C and the reaction monitored by IR spectroscopy. After 3 h, the IR spectrum showed the typical ν_{CO} absorptions of **8** and the reaction was stopped without any further work-up.

This item was downloaded from IRIS Università di Bologna (<https://cris.unibo.it/>)

When citing, please refer to the published version.

4.9 Thermal decomposition of Fe(CO)₄(AuIPr)(AuPPh₃) (7)

A solution of 7 (0.450 g, 0.371 mmol) in dmsO (15 mL) was heated at 130 °C and the reaction monitored by IR spectroscopy. After 5 h, the IR spectrum showed the typical ν_{CO} absorptions of the starting compound 7. The temperature was increased up to 150 °C without any clear evidence of decomposition.

4.10 X-ray Crystallographic Study.

Crystal data and collection details for [Au(IMes)₂][15]·0.67CH₂Cl₂, [Au(IPr)₂][16], [NEt₄]₂[9], [NEt₄][12], [17][BF₄]_n·solv and [NEt₄][11]·1.5toluene were reported in Table S5 in Supporting Information. The diffraction experiments were carried out on a Bruker APEX II diffractometer equipped with a CCD ([17][BF₄]_n·solv) or a PHOTON100 ([Au(IMes)₂][15]·0.67CH₂Cl₂, [Au(IPr)₂][16], [NEt₄]₂[9], [NEt₄][12], [NEt₄][11]·1.5toluene) detector using Mo–K α radiation. Data were corrected for Lorentz polarization and absorption effects (empirical absorption correction SADABS).⁵³ Structures were solved by direct methods and refined by full-matrix least-squares based on all data using F^2 .⁵⁴ Hydrogen atoms were fixed at calculated positions and refined by a riding model. All non-hydrogen atoms were refined with anisotropic displacement parameters, unless otherwise stated.

[Au(IMes)₂][15]·0.67CH₂Cl₂: The asymmetric unit of the unit cell contains one cluster anion located on a general position, half of a cluster anion located on an inversion centre, one [Au(IMes)₂]⁺ cation located on a general position, half of a [Au(IMes)₂]⁺ cation located on an inversion centre, and one CH₂Cl₂ molecule located on a general position. The CO ligands of the cluster anion located on an inversion centre as well as the IMes ligands of the [Au(IMes)₂]⁺ cation located on an inversion centre are disordered. Thus, they have been split into two positions and refined using one occupancy factor per disordered group. The disordered CO ligands and the CH₂Cl₂ molecule have been refined isotropically. All C, N and O atoms have been restrained to have similar U parameters (SIMU line in SHELXL, s.u. 0.01) and to isotropic behaviour (ISOR line in SHELXL, s.u. 0.01). All the aromatic C-atoms have been constrained to fit regular hexagons (AFIX 66 line in SHELXL). Mainly because of the disorder issues mentioned above, the refined R_1 factor was 0.1276.

[Au(IPr)₂][16]: The asymmetric unit of the unit cell contains half of a [HFe(CO)₄][−] anion and half of a [Au(IPr)₂]⁺ cation both located on 2-fold axis. The N and C atoms of the IPr ligands have been

This item was downloaded from IRIS Università di Bologna (<https://cris.unibo.it/>)

When citing, please refer to the published version.

restrained to have similar U parameters (SIMU line in SHELXL, s.u. 0.02). The $[\text{HFe}(\text{CO})_4]^-$ anion is disordered over two equally populated and symmetry related positions. Because of this disorder, it has not been possible to locate the hydride ligand.

[NEt₄]₂[9]: The asymmetric unit of the unit cell contains two cluster anions and four $[\text{NEt}_4]^+$ cations located on general positions. The crystals are racemically twinned with refined batch factor 0.32(2). Two $[\text{NEt}_4]^+$ cations are disordered and, thus, they have been split into two positions each and refined anisotropically with one occupancy factor per disordered unit. The disordered cations have been restrained to have similar U parameters (SIMU line in SHELXL, s.u. 0.01), similar geometries (SAME line in SHELXL, s.u. 0.02) and isotropic behaviour (ISOR line in SHELXL, s.u. 0.01).

[NEt₄][12]: The asymmetric unit of the unit cell contains one cluster anion and one $[\text{NEt}_4]^+$ cation both located on general positions.

[17][BF₄]_n·solv: The asymmetric unit of the unit cell contains one fourth of a cluster molecule located on $\bar{4}$. A total potential solvent accessible void of 1794 Å³ (ca. 22% of the Cell Volume) remain within the unit cell after refinement. These voids are organized in infinite channels parallel to the crystallographic c axis. In view of the fact that the crystals are very small, even if the data have been collected at 100 K with 120 s per frame, it has not been possible to crystallographically identify any molecule within these channels. For the same reasons, the final R_1 factor was 0.1799. It must be remarked that, even if hundreds of Fourier peaks are included during refinement (PLAN 200 or even higher in SHELXL), all of them are located close to the cluster molecule and not within the void channels. In addition, ¹H and ¹³C NMR analyses of the crystals dissolved in d₆-acetone did not show any significant peaks apart those attributable to the cluster molecule. Conversely, ¹⁹F NMR analyses clearly pointed out the presence of $[\text{BF}_4]^-$ anions. Nonetheless, since it was not possible to locate and refine such anions within the crystal structure, these voids were treated using the SQUEEZE routine of PLATON.⁵⁵ All phenyl rings have been constrained to fit regular hexagons (AFIX 66 line in SHELXL).

[NEt₄][11]·1.5toluene: The asymmetric unit of the unit cell contains one cluster anion located on a general position, one $[\text{NEt}_4]^+$ cation located on a general position, one toluene molecule located on a general position and one toluene molecule located on an inversion centre disordered over two symmetry related positions (occupancy factor 0.5). All the C, O and N atoms have been restrained to have similar U parameters (SIMU line in SHELXL, s.u. 0.01). The C-N and C-C distances of the $[\text{NEt}_4]^+$ cation have been restrained to be similar (SADI line in SHELXL, s.u. 0.02). The aromatic

This item was downloaded from IRIS Università di Bologna (<https://cris.unibo.it/>)

When citing, please refer to the published version.

rings of the toluene molecules have been constrained to fit regular hexagons (AFIX 66 line in SHELXL) and all the C-atoms of the toluene molecules have been restrained and to isotropic behaviour (ISOR line in SHELXL, s.u. 0.01). The overall quality of the crystals was rather low, leading to a final R_1 factor of 0.2778.

4.11 Computational details

Geometry optimizations of the clusters **10**, **11**, **15a** and **15b** were performed in gas phase using the range-separated hybrid DFT functional ω B97X.⁵⁶ The basis set used was the Ahlrichs' def2 split-valence, with polarization and diffusion functions and relativistic ECP for Au.⁵⁷ Single point calculations on the optimized structures of **10**, **11**, **15a** and **15b** and on the models for compound **17** were carried out at the same theoretical level, including non-local correlation by the VV10 functional (wB97X-v).⁵⁸ Geometry optimizations of **3**, **8** and **13** were carried out using the PBEh-3c method, which is a reparameterized version of PBE0 (with 42 % HF exchange) that uses a split-valence double-zeta basis set (def2-mSVP) and adds three corrections that consider dispersion, basis set superposition and other basis set incompleteness effects.⁵⁹ The C-PCM solvation model was added to PBEh-3c calculations,⁶⁰ considering a dielectric constant of 41.7 and a refractive index of 1.45544, intermediate between the values reported for dmso and dmf. The "restricted" approach was used in all the cases. Calculations were performed with the ORCA 4.0.1.2.⁶¹ The output, converted in .molden format, was used for AIM and Hirshfeld analyses,⁶² performed with the software Multiwfn, version 3.5.⁶³ Cartesian coordinates of the DFT-optimized structures are collected in a separated .xyz file.

ASSOCIATED CONTENT

Supporting Information

The Supporting Information is available free of charge on the ACS Publications website.

Crystallographic data in CIF format. NMR spectra. Crystals and experimental details. Optimized coordinates in XYZ format (XYZ).

Accession Codes

CCDC 1955604-1955609 contain the supplementary crystallographic data for this paper. These data can be obtained free of charge via www.ccdc.cam.ac.uk/data_request/cif, or by emailing

This item was downloaded from IRIS Università di Bologna (<https://cris.unibo.it/>)

When citing, please refer to the published version.

data_request@ccdc.cam.ac.uk, or by contacting The Cambridge Crystallographic Data Centre, 12, Union Road, Cambridge CB2 1EZ, UK; fax: +44 1223 336033.

AUTHOR INFORMATION

Corresponding Author

* E-mail: stefano.zacchini@unibo.it. Tel: +39 051 2093711. Web: <https://www.unibo.it/sitoweb/stefano.zacchini/en>.

Notes

The authors declare no competing financial interest.

ACKNOWLEDGMENTS

We thank the University of Bologna for financial support. We thank the referees for the useful suggestions in revising the manuscript.

REFERENCES

- (1) Ciabatti, I.; Femoni, C.; Iapalucci, M. C.; Ruggieri, S.; Zacchini, S. The role of gold in transition metal carbonyl clusters. *Coord. Chem. Rev.* **2018**, *355*, 27-38.
- (2) (a) Coffey, C. F.; Lewis, J.; Nyholm, R. S. Metal-Metal Bonds. Part I. Compounds of Gold(0) with the Carbonyls of Manganese, Iron, and Cobalt. *J. Chem. Soc.* **1964**, 1741-1749. (b) Albano, V. G.; Monari, M.; Iapalucci, M. C.; Longoni, G. Structural characterization of the trinuclear cluster compound $[\text{Fe}(\text{CO})_4(\text{AuPPh}_3)_2]$ and isolation of its parent anion $[\text{Fe}(\text{CO})_4(\text{AuPPh}_3)]^-$. *Inorg. Chim. Acta* **1993**, *213*, 183-190.
- (3) Bortoluzzi, M.; Cesari, C.; Ciabatti, I.; Femoni, C.; Hayatifar, M.; Iapalucci, M. C.; Mazzoni, R.; Zacchini, S. Bimetallic Fe-Au Carbonyl Clusters Derived from Collman's Reagent: Synthesis, Structure and DFT Analysis of $\text{Fe}(\text{CO})_4(\text{AuNHC})_2$ and $[\text{Au}_3\text{Fe}_2(\text{CO})_8(\text{NHC})_2]^-$. *J. Clust. Sci.* **2017**, *28*, 703-723.
- (4) Berti, B.; Bortoluzzi, M.; Cesari, C.; Femoni, C.; Iapalucci, M. C.; Mazzoni, R.; Vacca, F.; Zacchini, S. Synthesis and Characterization of Heterobimetallic Carbonyl Clusters with Direct Au-Fe and Au...Au Interactions supported by N-Heterocyclic Carbene and Phosphine Ligands. *Eur. J. Inorg. Chem.* **2019**, 3084-3093.

This item was downloaded from IRIS Università di Bologna (<https://cris.unibo.it/>)

When citing, please refer to the published version.

- (5) Albano, V. G.; Castellari, C.; Iapalucci, M. C.; Longoni, G.; Monari, M.; Paselli, A.; Zacchini, S. Synthesis, chemical characterization and molecular structure of $[\text{Ag}_3\{\mu_3\text{-Fe}(\text{CO})_4\}(\text{dppm})_3][\text{NO}_3]$ and $[\text{Au}_3\{\mu\text{-Fe}(\text{CO})_4\}(\text{dppm})_2][\text{Cl}]$. *J. Organomet. Chem.* **1999**, *573*, 261-266.
- (6) Albano, V. G.; Iapalucci, M. C.; Longoni, G.; Manzi, L.; Monari, M. Synthesis of $[\text{Au}_3\text{Fe}_2(\text{CO})_8(\text{dppm})]^-$ and $[\text{Au}_5\text{Fe}_2(\text{CO})_8(\text{dppm})_2]^+$: X-ray Structures of $[\text{NET}_4][\text{Au}_3\text{Fe}_2(\text{CO})_8(\text{dppm})]$ and $[\text{Au}_5\text{Fe}_2(\text{CO})_8(\text{dppm})_2][\text{BF}_4]$. *Organometallics* **1997**, *16*, 497-499.
- (7) Berti, B.; Bortoluzzi, M.; Cesari, C.; Femoni, C.; Iapalucci, M. C.; Mazzoni, R.; Vacca, F.; Zacchini, S. Polymerization Isomerism in $[\{\text{MFe}(\text{CO})_4\}_n]^{n-}$ (M = Cu, Ag, Au; N = 3, 4) Molecular Cluster Supported by Metallophilic Interactions. *Inorg. Chem.* **2019**, *58*, 2911-2915.
- (8) Albano, V. G.; Calderoni, F.; Iapalucci, M. C.; Longoni, G.; Monari, M. Synthesis of $[\text{AuFe}_2(\text{CO})_8]^{3-}$ and $[\text{Au}_4\text{Fe}_4(\text{CO})_{16}]^{4-}$: X-ray structure of the $[\text{Au}_4\text{Fe}_4(\text{CO})_{16}]^{4-}$ cluster anion in its $[\text{NET}_4]^+$ salt. *Chem. Commun.* **1995**, 433-434.
- (9) Femoni, C.; Iapalucci, M. C.; Longoni, G.; Tiozzo, C.; Zacchini, S. An Organometallic Approach to Gold Nanoparticles: Synthesis and X-Ray Structure of CO-Protected $\text{Au}_{21}\text{Fe}_{10}$, $\text{Au}_{22}\text{Fe}_{12}$, $\text{Au}_{28}\text{Fe}_{14}$, and $\text{Au}_{34}\text{Fe}_{14}$ Clusters. *Angew. Chem. Int. Ed.* **2008**, *47*, 6666-6669.
- (10) Albano, V. G.; Castellari, C.; Femoni, C.; Iapalucci, M. C.; Longoni, G.; Monari, M.; Zacchini, S. Synthesis, Chemical Characterization, and Molecular Structure of $\text{Au}_8\{\text{Fe}(\text{CO})_4\}_4(\text{dppe})_2$ and $\text{Au}_6\text{Cu}_2\{\text{Fe}(\text{CO})_4\}_4(\text{dppe})_2$. *J. Clust. Sci.* **2001**, *12*, 75-87.
- (11) Zacchini, S. Using Metal Carbonyl Clusters To Develop a Molecular Approach towards Metal Nanoparticles. *Eur. J. Inorg. Chem.* **2011**, 4125-4145.
- (12) Jadzinsky, P. D.; Calero, G.; Ackerson, C. A.; Bushnell, D. A.; Kornberg, R. D. Structure of a Thiol Monolayer-Protected Gold Nanoparticle at 1.1 Å Resolution. *Science* **2007**, *318*, 430-433.
- (13) Xu, W. W.; Zeng, X. C.; Gao, Y. The structural isomerism in gold nanoclusters. *Nanoscale* **2018**, *10*, 9476-9483.
- (14) (a) Qian, H.; Ecckenhoff, W. T.; Zhu, Y.; Pintauer, T.; Jin, R. Total Structure Determination of Thiolate-Protected Au_{38} Nanoparticles. *J. Am. Chem. Soc.* **2010**, *132*, 8280-8281. (b) Tian,

This item was downloaded from IRIS Università di Bologna (<https://cris.unibo.it/>)

When citing, please refer to the published version.

- S.; Li, Y.-Z.; Li, M.-B.; Yuan, J.; Yang, J.; Wu, Z.; Jin, R. Structural Isomerism in Gold Nanoparticles Revealed by X-Ray Crystallography. *Nat. Commun.* **2015**, *6*, 8667.
- (15) Jin, R.; Zeng, C.; Zhou, M.; Chen, Y. Atomically Precise Colloid Metal Nanoclusters and Nanoparticles: Fundamentals and Opportunities. *Chem. Rev.* **2016**, *116*, 10346-10413.
- (16) Chakraborty, I.; Pradeep, T. Atomically Precise Clusters of Noble Metals: Emerging Link between Atoms and Nanoparticles. *Chem. Rev.* **2017**, *117*, 8208-8271.
- (17) (a) Parker, J. F.; Fields-Zinna, C. A.; Murray, R. W. The Story of a Monodisperse Gold Nanoparticle: Au₁₅L₁₈. *Acc. Chem. Res.* **2010**, *43*, 1289-1296. (b) Maity, P.; Xie, S.; Yamauchi, M.; Tsukuda, T. Stabilized gold clusters: from isolation toward controlled synthesis. *Nanoscale* **2012**, *4*, 4027-4037.
- (18) (a) Yao, Q.; Chen, T.; Yuan, X.; Xie, J. Toward Total Synthesis of Thiolate-Protected Metal Nanoclusters. *Acc. Chem. Res.* **2018**, *51*, 1338-1348. (b) Takano, S.; Hasegawa, S.; Suyama, M.; Tsukuda, T. Hydride Doping of Chemically Modified Gold-Based Superatoms. *Acc. Chem. Res.* **2018**, *51*, 3074-3083.
- (19) Zhang, Y.; Zhang, C.; Xu, C.; Wang, X.; Liu, C.; Waterhouse, G. I. N.; Wang, Y.; Yin, H. Ultrasmall Au nanoclusters for biomedical and biosensing applications: A mini-review. *Talanta* **2019**, *200*, 432-442.
- (20) (a) Lei, Z.; Wan, X.-K.; Yuan, S.-F.; Guan, Z.-J.; Wang, Q.-M. Alkynyl Approach toward the Protection of Metal Nanoclusters. *Acc. Chem. Res.* **2018**, *51*, 2465-2474. (b) Konishi, K.; Iwasaki, M.; Shichibu, Y. Phosphine-Ligated Gold Clusters with Core+exo Geometries: Unique Properties and Interactions at the Ligand-Cluster Interface. *Acc. Chem. Res.* **2018**, *51*, 3125-3133.
- (21) Narouz, M. R.; Osten, K. M.; Unsworth, P. J.; Man, R. W. Y.; Salorinne, K.; Takano, S.; Tomihara, R.; Kaappa, S.; Malola, S.; Dinh, C.-T.; Padmos, J. D.; Ayoo, K.; Garrett, P. J.; Nambo, M.; Horton, J. H.; Sargent, E. H.; Häkkinen, H.; Tsukuda, T.; Crudden, C. M. N-heterocyclic carbene-functionalized magic-number gold nanoclusters. *Nature Chem.* **2019**, *11*, 419-425.
- (22) Kenzler, S.; Schrenk, C.; Frojd, A. R.; Häkkinen, H.; Clayborne, A. Z.; Schnepf, A. Au₇₀S₂₀(PPh₃)₁₂: an intermediate sized metalloid gold cluster stabilized by the Au₄A₄ ring motif and Au-PPh₃ groups. *Chem. Commun.* **2018**, *54*, 248-251.

This item was downloaded from IRIS Università di Bologna (<https://cris.unibo.it/>)

When citing, please refer to the published version.

- (23) Sculfort, S.; Braunstein, P. Intramolecular d^{10} - d^{10} interactions in heterometallic clusters of the transition metals. *Chem. Soc. Rev.* **2011**, *40*, 2741-2760.
- (24) (a) Croizat, P.; Sculfort, S.; Welter, R.; Braunstein, P. Hexa- and Octanuclear Heterometallic Clusters with Copper-, Silver-, or Gold-Molybdenum Bonds and d^{10} - d^{10} Interactions. *Organometallics* **2016**, *35*, 3949-3958. (b) Sculfort, S.; Croizat, P.; Messaoudi, A.; Bénard, M.; Rohmer, M.-M.; Welter, R.; Braunstein, P. Two-Dimensional Triangular and Square Heterometallic Clusters: Influence of the Closed-Shell d^{10} Electronic Configuration. *Angew. Chem. Int. Ed.* **2009**, *48*, 9663-9667.
- (25) Schmidbaur, H.; Schier, A. Auophilic interactions as a subject of current research: an update. *Chem Soc. Rev.* **2012**, *41*, 370-412.
- (26) (a) Al-Ani, F. T.; Hughes, D. L.; Pickett, C. J. From an $\{Fe_4S_4\}$ -cluster to $\{Fe_2S_2\}$ - and $\{Fe_3S\}$ -carbonyls. Crystal structure of $[Fe_3S(CO)_9]^{2-}$. *J. Organomet. Chem.* **1986**, *307*, C31-C34. (b) van Hal, J. W.; Whitmire, K. H. Site-Directed Alkylation of $[EFe(CO)_9]^{2-}$ (E = S, Se, Te) Mediated by the Chalcogenide. Synthesis, Spectroscopic Characterization, and Reactivity of $[PPN][MeFe_3(CO)_9E]$ (E = Se, Te). *Organometallics* **1998**, *17*, 5197-5201. (c) Zhigui, Z.; Lixin, W.; Hengbin, Z.; Ling, Y.; Yuguo, F. The synthesis, structure and redox properties of the $[Fe_3S(CO)_9]^{2-}$ dianion. *Eur. J. Solid State Inorg. Chem.* **1991**, *28*, 1269-1276.
- (27) Kotsinaris, A.; Kyriacou, G.; Lambrou, Ch. Electrochemical reduction of dichloromethane to higher hydrocarbons. *J. Appl. Electrochem.* **1998**, *28*, 613-616.
- (28) Rossell, O.; Seco, M.; Jones, P. G. Preparation and Crystal Structure of $(NEt_4)[Fe_2(CO)_8(\mu-AuPPh_3)]$. *Inorg. Chem.* **1990**, *29*, 348-350.
- (29) Deng, H.; Shore, S. G. Unusual Iron-Iron and Ruthenium-Ruthenium Single Bonds Doubly Bridged by Two $Cu(PR_3)$ Fragments: Syntheses of Iron-Copper, Iron-Silver, and Ruthenium-Copper Heterometallic Complexes and Structures of $M_2(CO)_8(\mu-CuPCy_3)_2$ (M = Fe, Ru), $[PPh_4][Fe_2(CO)_8(\mu-CuPCy_3)]$, and $[PPh_4]_2\{[Fe_2(CO)_8]_2[\mu_4-\eta^2-Cu_2(Cy_2PCH_2CH_2PCy_2)]\}$. *Organometallics* **1991**, *10*, 3486-3498.
- (30) (a) Lagrone, C. B.; Whitmire, K. H.; Churchill, M. R.; Fettinger, J. C. Synthesis and Characterization of an Iron Carbonyl Cluster Containing Lead: Crystal and Molecular Structure of $[Et_4N]_2[Pb\{Fe(CO)_4\}_2\{Fe_2(CO)_8\}]$. *Inorg. Chem.* **1986**, *25*, 2080-2085. (b) Whitmire, K. H.; Shieh, M.; Cassidy, J. M. Synthesis, Characterization, and Reactivity of Iron Carbonyl Clusters Containing Bismuth or Antimony. Crystal Structures of Isomorphous

This item was downloaded from IRIS Università di Bologna (<https://cris.unibo.it/>)

When citing, please refer to the published version.

- [Et₄N][BiFe₃Cr(CO)₁₇] and [Et₄N][SbFe₃Cr(CO)₁₇] and Ring Complex Bi₂Fe₂(CO)₈Me₂. *Inorg. Chem.* **1989**, *28*, 3164-3170.
- (31) (a) Cassidy, J. M.; Whitmire, K. H.; Kook, A. M. Solution dynamics of tin and lead iron carbonyl compounds and the solid state structure of [Et₄N]₂[Sn{Fe₂(CO)₈}{Fe(CO)₄}]₂. *J. Organomet. Chem.* **1993**, *456*, 61-70. (b) Guzman-Jimenez, I. Y.; Whitmire, K. H. Bis(tetraethylammonium) tetra-μ-carbonyl-icosacarbonylhexairondithallate(2 Fe-Fe)(8 Fe-Tl)(2-). *Acta Cryst.* **1998**, *C54*, IUC9800053.
- (32) Cotton, F. A.; Troup, J. M. Accurate determination of a classic structure in the metal carbonyl field: nonacarbonyldi-iron. *J. Chem. Soc., Dalton Trans.* **1974**, 800-802.
- (33) Lourdichi, M.; Mathieu, R. Reactivity of [HFe₃(CO)₁₁]⁻ toward Alkynes. 1. Case of acetylene. *Organometallics* **1986**, *5*, 2067-2071.
- (34) Brun, P.; Dawkins, G. M.; Green, M.; Mills, R. M.; Salaun, J.-Y.; Stone, F. G. A.; Woodward, P. Conversion of a Bridged Vinylalkylidene Complex into Cluster Complexes of Cobalt, Iron, and Manganese: X-Ray Crystal Structures of [Fe₃(CO)₆(μ-CO)(μ₃-CMe)(η-C₅H₅)] and [FeCo₃(CO)₇(μ-CO)₂(μ₄-C=CH₂)(η-C₅H₅)]. *J. Chem. Soc., Chem. Commun.* **1981**, 966-968.
- (35) Wong, K. S.; Haller, K. J.; Dutta, T. K.; Chipman, D. M.; Fehlner, T. P. Effects of Bridging Hydrogens on Metal-Metal Bonds. 1. Geometrical Comparison of Fe₃(μ-H)₃(CO)₉(μ₃-CCH₃), Co₃(CO)₉(μ₃-CCH₃), and Model Compounds. *Inorg. Chem.* **1982**, *21*, 3197-3202.
- (36) Wong, W. K.; Chiu, K. W.; Wilkinson, G.; Galas, A. M. R.; Thornton-Pett, M.; Hursthouse, M. B. Electrophilic Attack on the [μ₃-acetyl-C¹(Fe¹:Fe²)O(Fe¹:Fe³)] nonacarbonyl-triangulo-triferrate(1-) anion by fluoroboric acid and methyl fluorosulphate. Carbon-oxygen bond cleavage to give μ₃-ethynidyne and μ-methoxy-groups. X-Ray crystal structures of Fe₃(CO)₉(μ₃-MeCO)(μ-H), Fe₃(CO)₉(μ₃-CMe)(μ₃-OMe), and Fe₃(CO)₉(μ₃-CMe)(μ₃-COMe). *J. Chem. Soc., Dalton Trans.* **1983**, 1557-1563.
- (37) Attali, S.; Dahan, F.; Mathieu, R. The [Fe₃(μ₃-CR)(CO)₁₀]⁻ Cluster Anions as Building Blocks for the Synthesis of Mixed-metal Clusters. Part 1. Synthesis of Mixed Clusters [MFe₃(μ₃-CMe)(CO)₁₀(PPh₃)] (M = Cu or Au) and Crystals Structure of [CuFe₃(μ₃-CMe)(CO)₁₀(PPh₃)]. *J. Chem. Soc., Dalton Trans.* **1985**, 2521-2524.
- (38) (a) Holt, E. M.; Whitmire, K. H.; Shriver, D. F. Nucleophilic Attack and Structural Rearrangements in Some Iron Carbonyl Cluster Carbides. Syntheses, Structures, and Reactions of the Tetrahedral Four-Iron Clusters [Fe₄(CO)₁₂(μ₃-COCH₃)]⁻ and

This item was downloaded from IRIS Università di Bologna (<https://cris.unibo.it/>)

When citing, please refer to the published version.

- $[\text{Fe}_4(\text{CO})_{12}(\text{CCH}_3)]^-$. *J. Am. Chem. Soc.* **1982**, *104*, 5621-5626. (b) Femoni, C.; Iapalucci, M. C.; Longoni, G.; Zacchini, S. The chemistry of hydridocarbonylferrates revisited: syntheses and structures of the new $[\text{H}_2\text{Fe}_4(\text{CO})_{12}]^{2-}$ and $[\text{HFe}_5(\text{CO})_{14}]^{3-}$ anions, and the $[\text{Fe}(\text{DMF})_4][\text{Fe}_4(\text{CO})_{12}(\mu_5-\eta^2-\text{CO})(\mu-\text{H})]_2$ adduct containing an unprecedented isocarbonyl. *Dalton Trans.* **2011**, *40*, 8685-8694.
- (39) (a) Kolis, J. W.; Holt, E. M.; Drezdson, M.; Whitmire, K. H.; Shriver, D. F. A Reactive Three-Metal Carbide Cluster Mimic, $[\text{Fe}_3(\text{CO})_9(\text{CCO})]^{2-}$. *J. Am. Chem. Soc.* **1982**, *104*, 6134-6135. (b) Kolis, J. W.; Holt, E. M.; Shriver, D. F. Synthesis, X-ray Crystal Structure, and Chemistry of a Metal Cluster Ketenylidene, $[\text{Fe}_3(\text{CO})_9(\text{CCO})]^{2-}$, with Carbide-like Reactivity. *J. Am. Chem. Soc.* **1983**, *105*, 7307-7313.
- (40) Mendizabal, F.; Miranda-Rojas, S.; Barrientos-Poblete, L. A comparative study between post-Hartree-Fock methods and density functional theory in closed-shell aurophilic attraction. *Comput. Theor. Chem.* **2015**, *1057*, 74-79.
- (41) (a) Bianchi, R.; Gervasio G.; Marabello, D. Experimental Electron Density Analysis of $\text{Mn}_2(\text{CO})_{10}$: Metal-Metal and Metal-Ligand Bond Characterization. *Inorg. Chem.*, **2000**, *39*, 2360-2366. (b) Lepetit, C.; Fau, P.; Fajerweg, K.; Kahn M. L.; Silvi, B. Topological analysis of the metal-metal bond: A tutorial review. *Coord. Chem. Rev.*, **2017**, *345*, 150-181.
- (42) Smith, M. B.; Bau, R. Structure of the $[\text{HFe}(\text{CO})_4]^-$ Anion. *J. Am. Chem. Soc.* **1973**, *95*, 2388-2389.
- (43) Chakrahari, K. K.; Silalahi, R. P. B.; Liao, J.-H.; Kahlal, S.; Liu, Y.-C.; Lee, J.-F.; Chiang, M.-H.; Sailard, J.-Y.; Liu, C. W. Synthesis and structural characterization from a two-electron superatomic copper nanocluster. *Chem. Sci.* **2018**, *9*, 6785-6795.
- (44) (a) Cordero, B.; Gómez, V.; Platero-Prats, A. E.; Revés, M.; Echeverría, J.; Cremades, E.; Barrágan, F.; Alvarez, S. Covalent radii revisited. *Dalton Trans.* **2008**, 2832-2838. (b) Bondi, A. Van der Waals Volumes and Radii. *J. Phys. Chem.* **1964**, *68*, 441-451.
- (45) (a) Gan, Z.; Chen, J.; Wuang, J.; Wang, C.; Li, M.-B.; Yao, C.; Zhuang, S.; Xu, A.; Li, L.; Wu, Z. The fourth crystallographic closest packing unveiled in the gold nanocluster crystal. *Nat. Commun.* **2017**, *8*, 14739. (b) Teo, P.; Koh, L. L.; Hor, T. S. A. Assembly of gold rings and chains with pyridyl carboxylates as directional spacer. *Chem. Commun.* **2007**, 2225-2227. (c) Canales, F.; Gimeno, M. C.; Jones, P. G.; Laguna, A. Aurophilicity at Sulfur Centers:

This item was downloaded from IRIS Università di Bologna (<https://cris.unibo.it/>)

When citing, please refer to the published version.

Synthesis and Structure of the Tetragold(I) Species $[(PPh_3Au)_4S](CF_3SO_3)_2 \cdot 2CH_2Cl_2$. *Angew. Chem. Int. Ed.* **1994**, *33*, 769-770.

- (46) (a) Canales, F.; Gimeno, M. C.; Laguna, A.; Jones, P. G. Auophilicity at Sulfur Centers. Synthesis and Reactivity of the Complex $[S(Au_2dppf)]$: Formation of Polynuclear Sulfur-Centered Complexes. Crystal Structures of $[S(Au_2dppf)] \cdot 2CHCl_3$, $[(\mu-Au_2dppf)\{S(Au_2dppf)\}_2](OTf)_2 \cdot 8CHCl_3$, and $[S(AuPPh_2Me)_2(Au_2dppf)](ClO_4)_2 \cdot 3CH_2Cl_2$. *J. Am. Chem. Soc.* **1996**, *118*, 4839-4845. (b) Yu, W.; Fuhr, O.; Fenske, D. Derivatives of Bis(diphenylphosphino)maleic Anhydride as Ligands in Polynuclear Gold(I) Complexes. *J. Clust. Sci.* **2012**, *23*, 753-766.
- (47) Zhou, S.; Pei, W.; Du, Q.; Zhao, J. Foreign atom encapsulated Au_{12} golden cages for catalysis of CO oxidation. *Phys. Chem. Chem. Phys.* **2019**, *21*, 10587-10593.
- (48) Albano, V. G.; Calderoni, F.; Iapalucci, M. C.; Longoni, G.; Monari, M.; Zanello, P. Synthesis, Chemical, and Electrochemical Characterization of the $[Ag_{13}\{\mu_3-Fe(CO)_4\}_8]^{n-}$ (n = 3, 4, 5) Cluster Anions: X-Ray Structural Determination of $[N(PPh_3)_2]_3[Ag_{12}(\mu_{12}-Ag)\{\mu_3-Fe(CO)_4\}_8]$. *J. Clust. Sci.* **1995**, *6*, 107-123.
- (49) Mingos, D. M. P.; May, A. S. In *Chemistry of Metal Cluster Complexes*. Shriver, D. S.; Kaesz, H. D.; Adams, R. D., Eds. VCH, **1990**.
- (50) Muetterties, E. L.; Stein, J. Mechanistic Features of Catalytic Carbon Monoxide Hydrogenation Reactions. *Chem Rev.* **1979**, *79*, 479-490.
- (51) (a) Churchill, M. R.; Wormald, J.; Knight, J.; Mays, M. J. Synthesis and Crystallographic Characterization of $[Me_4N^+]_2[Fe_6(CO)_{16}C^{2-}]$, a Hexanuclear Carbido-carbonyl Derivative of Iron. *J. Am. Chem. Soc.* **1971**, *93*, 3073-3074. (b) Churchill, M. R.; Wormald. Crystal and molecular structure of tetramethylammonium carbido-hexadecacarbonylhexaferrate(2-), $[Me_4N]_2[Fe_6(CO)_{16}C]$, a hexanuclear iron cluster complex with an encapsulated six-coordinate carbon atom. *J. Chem. Soc., Dalton Trans.* **1974**, 2410-2415.
- (52) Keller, E. *SCHAKAL99*; University of Freiburg: Germany, 1999.
- (53) Sheldrick, G. M. *SADABS-2008/1 - Bruker AXS Area Detector Scaling and Absorption Correction*; Bruker AXS: Madison, WI, 2008.
- (54) Sheldrick, G. M. Crystal Structure Refinement with SHELXL. *Acta Cryst.* **2015**, *C71*, 3-8.

This item was downloaded from IRIS Università di Bologna (<https://cris.unibo.it/>)

When citing, please refer to the published version.

- (55) (a) Spek, A. L. Single-crystal structure validation with the program *PLATON*. *J. Appl. Cryst.* **2003**, *36*, 7-13. (b) Spek, A. L. Structure validation in chemical crystallography. *Acta Cryst.* **2009**, *D65*, 148-155.
- (56) (a) Minenkov, Yu.; Singstad, Å.; Occhipinti, G.; Jensen, V. R. The accuracy of DFT-optimized geometries of functional transition metal compounds: a validation study of catalysts for olefin metathesis and other reactions in the homogeneous phase. *Dalton Trans.* **2012**, *41*, 5526-5541. (b) Chai, J.-D.; Head-Gordon, M. Long-range corrected hybrid density functionals with damped atom-atom dispersion corrections. *Phys. Chem. Chem. Phys.* **2008**, *10*, 6615-6620. (c) Gerber, I. C.; Ángyán, J. G. Hybrid functional with separated range. *Chem. Phys. Lett.* **2005**, *415*, 100-105.
- (57) (a) Weigend, F.; Ahlrichs, R. Balanced basis sets of split valence, triple zeta valence and quadruple zeta valence quality for H to Rn: Design and assessment of accuracy. *Phys. Chem. Chem. Phys.* **2005**, *7*, 3297-3305. (b) Andrae, D.; Häußermann, U.; Dolg, M.; Stoll, H.; Preuß, H. Energy-adjusted ab initio pseudopotentials for the second and third row transition elements. *Theor. Chim. Acta* **1990**, *77*, 123-141.
- (58) Mardirossian, N.; Head-Gordon, M. ω B97X-V: A 10-parameter, range-separated hybrid, generalized gradient approximation density functional with nonlocal correlation, designed by a survival-of-the-fittest strategy. *Phys. Chem. Chem. Phys.* **2014**, *16*, 9904-9924.
- (59) Grimme, S. Brandenburg, J. G.; Bannwarth, C.; Hansen, A. Consistent structures and interactions by density functional theory with small atomic orbital basis sets *J. Chem. Phys.* **2015**, *143*, 054107.
- (60) (a) Cossi, M.; Rega, N.; Scalmani, G.; Barone, V. Energies, structures, and electronic properties of molecules in solution with the C-PCM solvation model. *J. Comput. Chem.* **2003**, *24*, 669-681. (b) Barone, V.; Cossi, M. Quantum Calculation of Molecular Energies and Energy Gradients in Solution by a Conductor Solvent Model. *J. Phys. Chem. A* **1998**, *102*, 1995-2001.
- (61) (a) Neese, F. The ORCA program system. *WIREs Comput. Mol. Sci.* **2012**, *2*, 73-78. (b) Neese, F. Software update: the ORCA program system, version 4.0. *WIREs Comput. Mol. Sci.* **2018**, *8*, e1327.

This item was downloaded from IRIS Università di Bologna (<https://cris.unibo.it/>)

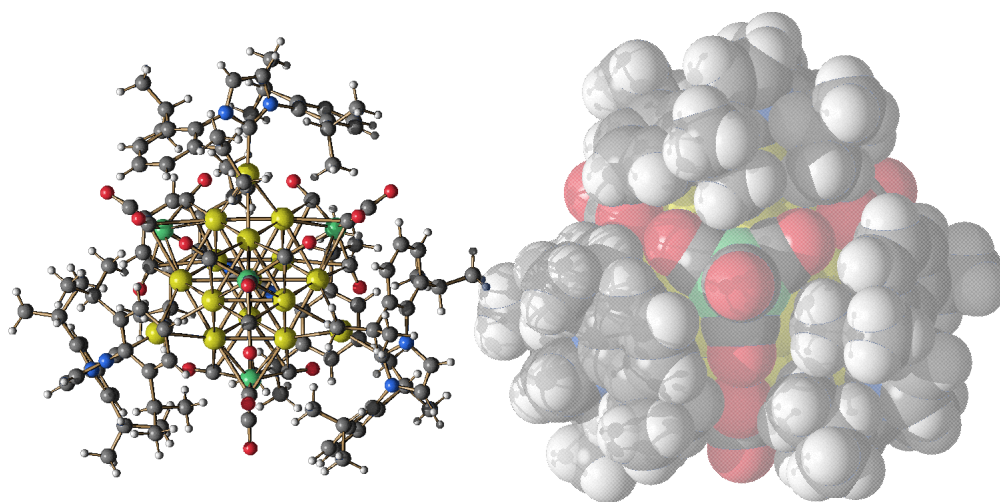
When citing, please refer to the published version.

- (62) (a) Cramer, C. J. *Essentials of Computational Chemistry*, second ed., Wiley, Chichester, 2004. (b) Hirshfeld, F. L. Bonded-atom fragments for describing molecular charge densities. *Theor. Chim. Acta* **1977**, *44*, 129-138.
- (63) Lu, T.; Chen, F. Multiwfn: A multifunctional wavefunction analyzer. *J. Comput. Chem.* **2012**, *33*, 580-592.

This item was downloaded from IRIS Università di Bologna (<https://cris.unibo.it/>)

When citing, please refer to the published version.

Table of contents



The nuclearity of Au-Fe molecular clusters has been increased by thermal methods resulting in heterometallic species stabilized by CO, NHC and phosphine ligands.

This item was downloaded from IRIS Università di Bologna (<https://cris.unibo.it/>)

When citing, please refer to the published version.